Amphiphilic peptide-tagged N-cadherin forms radial glial-like fibers that enhance neuronal migration in injured brain and promote sensorimotor recovery

Yuya Ohno[a,b,1], Chikako Nakajima[a,1], Itsuki Ajioka[c,d], Takahiro Muraoka[d,e], Atsuya Yaguchi[e], Teppei Fujioka[b], Saori Akimoto[c,d], Misaki Matsuo[a], Ahmed Lotfy[f], Sayuri Nakamura[a], Vicente Herranz-Pérez[g], José Manuel García-Verdugo[g], Noriyuki Matsukawa[b], Naoko Kaneko[a,h,*], Kazunobu Sawamoto[a,i,**]

[a] *Department of Developmental and Regenerative Neurobiology, Institute of Brain Science, Nagoya City University Graduate School of Medical Sciences, Nagoya, Aichi 467-8601, Japan*

[b] *Department of Neurology and Neuroscience, Nagoya City University Graduate School of Medical Sciences, Nagoya, Aichi 467-8601, Japan*

[c] *Center for Brain Integration Research (CBIR), Tokyo Medical and Dental University, Bunkyo-ku, Tokyo 113-8510, Japan*

[d] *Kanagawa Institute of Industrial Science and Technology (KISTEC), Kanagawa 243-0435, Japan*

[e] *Department of Applied Chemistry, Graduate School of Engineering, Tokyo University of Agriculture and Technology, Koganei, Tokyo 184-8588, Japan*

[f] *Biotechnology and Life Sciences Department, Faculty of Postgraduate Studies for Advanced Sciences (PSAS), Beni-Suef University, Beni-Suef, 62511, Egypt*

[g] *Laboratory of Comparative Neurobiology, Cavanilles Institute, University of Valencia, CIBERNED, 46980, Valencia, Spain*

[h] *Laboratory of Neuronal Regeneration, Graduate School of Brain Science, Doshisha University, Kyotanabe, Kyoto 610-0394, Japan*

[i] *Division of Neural Development and Regeneration, National Institute of Physiological Sciences, Okazaki, Aichi 444-8585, Japan*

[1] These authors contributed equally

* Corresponding author: Laboratory of Neuronal Regeneration, Graduate School of Brain Science, Doshisha University, 1-3 Tatara Miyakodani, Kyotanabe-shi, Kyoto 610-0394, Japan

** Corresponding author: Department of Developmental and Regenerative Neurobiology, Institute of Brain Science, Nagoya City University Graduate School of Medical Sciences, 1 Kawasumi, Mizuho-cho, Mizuho-ku, Nagoya, Aichi 467-8601, Japan

E-mail addresses: nkaneko@mail.doshisha.ac.jp (Naoko Kaneko), sawamoto@med.nagoya-cu.ac.jp (Kazunobu Sawamoto)

Running headline

N-cadherin-conjugated hydrogel promotes neuronal regeneration

Abstract

The mammalian brain has very limited ability to regenerate lost neurons and recover function after injury. Promoting the migration of young neurons (neuroblasts) derived from endogenous neural stem cells using biomaterials is a new and promising approach to aid recovery of the brain after injury. However, the delivery of sufficient neuroblasts to distant injured sites is a major challenge because of the limited number of scaffold cells that are available to guide neuroblast migration. To address this issue, we have developed an amphiphilic peptide [$(RADA)_3$-(RADG)] (mRADA)-tagged N-cadherin extracellular domain (Ncad-mRADA), which can remain in mRADA hydrogels and be injected into deep brain tissue to facilitate neuroblast migration. Migrating neuroblasts directly contacted the fiber-like Ncad-mRADA hydrogel and efficiently migrated toward an injured site in the striatum, a deep brain area. Furthermore, application of Ncad-mRADA to neonatal cortical brain injury efficiently promoted neuronal regeneration and functional recovery. These results demonstrate that self-assembling Ncad-mRADA peptides mimic both the function and structure of endogenous scaffold cells and provide a novel strategy for regenerative therapy.

Keywords

Self-assembling peptide, injectable hydrogel, scaffold material, neuronal migration, neuronal regeneration, ventricular-subventricular zone

Highlights

- A novel self-assembling Ncad-mRADA peptide forms a supramolecular hydrogel
- mRADA hydrogel incorporates the N-cadherin extracellular domain tagged with mRADA
- Ncad-mRADA hydrogel provides a scaffold for neuroblast migration in injured brain
- Migrating neuroblasts directly interact with radial-glial-like Ncad-mRADA fibers
- Ncad-mRADA promotes neuroblast migration and functional recovery after brain injury

Graphical abstract

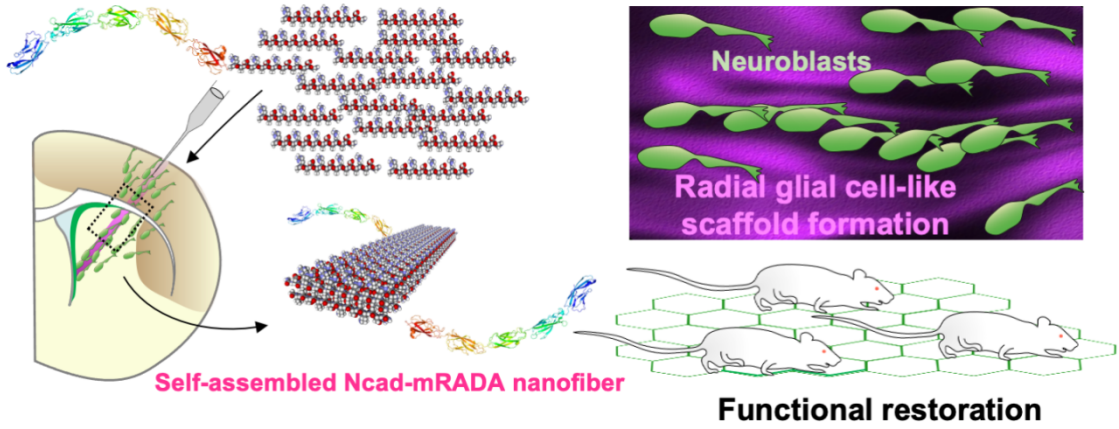

Introduction

Brain injury, such as stroke, causes significant loss of neurons, leading to a variety of irreversible neurological dysfunctions. To fundamentally treat brain injury, lost neurons need to be regenerated, but no such treatment exists. Biomaterials, which are biocompatible and biodegradable, show promise for promoting tissue repair. The use of biomaterials to deliver various regeneration-promoting factors (e.g., growth factors) to damaged tissues has recently been attempted for neuronal regeneration using neural stem cells (NSCs) [1–4].

In the postnatal mammal brain, NSCs reside within the ventricular-subventricular zone (V-SVZ) of the walls of the lateral ventricles, and have the ability to generate immature neurons [5,6]. In the rodent brain, these immature neurons (neuroblasts) form chain-like aggregates that enter the rostral migratory stream and migrate toward the olfactory bulb [7,8]. Upon injury, neural stem cells are activated to promote neuroblast production [9–11]. Neuroblasts are attracted by chemokines and migrate toward lesion sites [6]. Similar to the normal physiological state, neuroblasts in the injured brain utilize neighboring neuroblasts [12], blood vessels [12–15], and radial glial cells [16] as scaffolds for their migration. However, neuroblast migration is inhibited by reactive astrocytes hypertrophied by injury [17]. By promoting neuroblast migration, regenerated neurons are localized in appropriate positions, facilitating functional repair of the brain [17]. The use of neuroblasts derived from endogenous NSCs has the advantage of reducing tumorigenic risk associated with cell transplantation [18–20] and emerge as a safe and practical approach in regenerative medicine. Therefore, it is necessary to develop artificial scaffold materials that mimic the function and structure of the physiological scaffolds that facilitate the migration of endogenous neuroblasts.

We have previously reported that a porous sponge containing laminin, an extracellular matrix component of the basement membrane of blood vessels, transplanted into injured neonatal cortex promotes neuroblast migration [21]. We have also shown that sponges containing the extracellular domain of N-cadherin, a homophilic intercellular adhesion molecule expressed in radial glial cells and neuroblasts, promote the migration of neuroblasts that can differentiate into mature neurons and contribute to functional recovery [16]. While these studies indicate that sponges may be useful in the treatment of cortical lesions, there are limitations to the introduction of such solid materials into deep brain tissue, as their application is invasive and disrupts residual neuronal circuits. Neuronal regeneration in the deep brain requires minimally invasive materials, such as self-assembling peptides that form hydrogels when in contact with physiological fluids

[22–24]. We and other groups have reported that several injectable materials, such as laminin-mixed amphiphilic peptides $(RADA)_4$ [13], self-assembling peptides containing BDNF [25], and amphiphilic peptides incorporating Tenascin-C-mimetic short peptide [26], promote neuroblast migration when injected into the adult brain. The development of novel self-assembling peptides that form a hydrogel, characterized by a suitable scaffold structure for cell migration and the ability to more stably incorporate cell adhesion molecules, is needed to promote neuroblast migration in deep brain regions to effectively promote functional recovery.

We previously generated an amphiphilic peptide [$(RADA)_3$-(RADG)] (here referred to as mRADA) with reduced viscoelasticity compared with the original $(RADA)_4$ (here referred to as RADA) [27]. Here, we created a new material, the extracellular domain of N-cadherin tagged with an mRADA (Ncad-mRADA) that stably associates with mRADA hydrogels. The Ncad-mRADA-containing hydrogels promoted neuroblast migration and improvement in sensorimotor functions in mouse models of brain injury.

Materials and Methods

Animals

Wild-type Institute of Cancer Research (ICR) mice and were purchased from Japan SLC (Shizuoka, Japan). *Dcx-EGFP* mice [28] were obtained from the Mutant Mouse Research Resource Center (MMRRC. RRID: MMRRC_000244-MU). *NSE-DTA* transgenic mice [29] were obtained from S. Itohara. All experiments on live animals were performed in accordance with the ARRIVE guidelines, the U.K. Animals (Scientific Procedures) Act, 1986, the National Research Council's Guide for the Care and Use of Laboratory Animals, and the guidelines and regulations of Nagoya City University.

Peptide synthesis

RADA (Ac-RADARADARADARADA-NH_2) and mRADA (Ac-RADARADARADARADG-NH_2) were synthesized as previously reported [27]. For the synthesis of mRADA with selenomethionine (Ac-RADARADARADARADGSem-NH_2), Fmoc-Sem-OH was prepared by the following procedure. To an aqueous solution (5 mL) of seleno-L-methionine (0.188 g, 0.959 mmol, Nacalai Tesque, Kyoto, Japan) and $NaHCO_3$ (0.193 g, 2.30 mmol, Kishida Chemical, Tokyo, Japan) a 1,4-dioxane solution (10 mL, Kishida Chemical, Tokyo, Japan) of Fmoc-OSu (0.344 g, 1.02 mmol, Watanabe Chemical Industries, Hiroshima, Japan) was added dropwise over 90 min. After stirring

for 24 h at 25°C, 2 M HCl aq. was added to acidify the reaction mixture to pH 3. The reaction mixture was extracted with EtOAc (10 mL, three times), and the collected organic phase was washed with saturated NH_4Cl aq. (10 mL, once) and water (10 mL, twice). The organic phase was dried with Na_2SO_4. After filtration to remove insoluble substances, the organic phase was evaporated. The residue was separated on Sfär Silica HC D High Capacity Duo 20 μm using Isolera flash column chromatography of Biotage (Uppsala, Sweden) with a gradient elution between EtOAc and hexane (5/95 to 80/20) to isolate Fmoc-Sem-OH (0.245 g, 0.585 mmol) with 61% yield. JEOL ECX-400 ^{1}H NMR (400 MHz, $CDCl_3$) δ 8.19 (brs, 1H), 7.75 (d, J = 8.0 Hz, 2H), 7.61–7.50 (m, 2H), 7.39 (t, J = 7.5 Hz, 2H), 7.30 (t, J = 7.5 Hz, 2H), 5.44 (d, J = 8.6 Hz, 1H), 4.56–4.49 (m, 1H), 4.43 (d, J = 6.9 Hz, 1H), 4.22 (t, J = 6.9 Hz, 1H), 2.61–2.50 (m, 1H), 2.48–2.36 (m, 1H), 2.31–2.20 (m, 1H), 2.13–2.01 (m, 1H), 1.99 (s, 2H), 1.93 (s, 1H) ppm, JEOL ECX-400 ^{13}C NMR (125 MHz, $CDCl_3$) δ 176.69, 156.23, 143.87, 143.68, 141.43, 127.87, 127.19, 125.13, 120.14, 67.23, 53.94, 47.23, 32.75, 20.36, 4.36 ppm; Advion expression CMS-L ESI MS (MeOH, positive mode): m/z 420.1 (monoisotopic mass of $C_{20}H_{22}NO_4Se$ [M + H]$^+$: 420.07). mRADA with selenomethionine was synthesized following the same synthetic protocol as RADA and characterized by Bruker autoflex speed matrix-assisted laser desorption/ionization - time of flight mass spectrometry (2,5-dihydroxybenzoic acid, reflector positive mode): m/z 1877.85 (monoisotopic mass of $C_{70}H_{121}N_{30}O_{26}Se$ [M + H]$^+$: 1877.82).

EGFP-mRADA and Ncad-mRADA were created as below. To generate *pCAG-EGFP-6×Histag-A16G*, the *6×Histag-A16G* cDNA, attached *Not*I and *Xho*I sites were generated by annealing the DNA oligos, 5′-GGCCCATCATCAT CATCATCATCGAGCAGACGCCCGTGCGGATGCTAGAGCGGACGCCAGAGCA GATGGTTA-3′ and 5′-TCGAGTTAACCATCTGCTCTGGCGTCCGCTCTAGCATCCGCACGGGCGTCTG CTCGATGATGATGATGATGATG-3′, followed by insertion into the *Not*I/*Xho*I sites of *pCAG-EGFP-6×Histag* [30]. To generate a universal *pCAG-CST-6×Histag-A16G* plasmid, from which desirable A16G-tagged proteins can be easily generated, the cDNA encoding *6×Histag-A16G* was amplified from *pCAG-EGFP-6×Histag-A16G* using the following primers 5′-AAGCGGCCGCCATCATCATCATCATCATCG-3′ and 5′-CAGCTATGACCATGATTACGCC-3’ and then inserted into the *Not*I site of *pCAG-CST-HA* [31]. To generate *pCAG-Ncad-Fc-6×Histag-A16G*, we amplified the cDNA encoding *Ncad-Fc-6×Histag* from *pRc/CMV-Ncad-Fc* [32] using the following primers 5′-AAGCTAGCCATGTGCCGGATAGCGGGAG-3′ and 5′-AACTCGAGTTAATGATGATGATGATGATGTCTAGATTTACCAGGAGAGTGG GAGA-3′. Then the amplicon was inserted into the *Not*I/*Xho*I sites of *pCAG-CST-*

6×Histag-A16G. To generate *pCAG-Ncad-6×Histag-A16G*, we obtained the cDNA encoding the *Ncad* by *Nhe*I/*Not*I digestion and inserted it into *pCAG-CST-6×Histag-A16G*.

To obtain genetically engineered proteins, 293T cells (5.2×10^5 cells) were plated in 6-well plates in 2.5 mL Dulbecco's modified Eagle's medium containing 10% fetal bovine serum (FBS). One day later, the cells were transiently transfected with *pCAG-EGFP-6×Histag*, *pCAG-EGFP-6×Histag-A16G*, or *pCAG-Ncad-6×Histag-A16G* using TransIT-LT1 Transfection Reagent according to the manufacturer's instructions. To obtain Ncad-mRADA, the conditioned medium was collected at 7 days after transfection, passed through a 0.45-μm filter, concentrated using an ultrafiltration column (Amicon Ultra 10K; Merck, Darmstadt, Germany), displaced in phosphate buffer (PB, pH 7.4), and kept at −80°C before use. To obtain EGFP-mRADA and non-tagged EGFP, transfected 293T cells were lysed in lysis buffer [20 mM Tris (pH 7.4), 150 mM NaCl, 1 mM ethylene-diamine-tetra-acetic acid (EDTA), 1% NP-40, and protease inhibitor (Complete EDTA-free)], and the samples were centrifuged at 15,000 ×g for 5 min. The soluble fraction was concentrated using an ultrafiltration column (Amicon Ultra 10K, Merck), displaced in PB (pH 7.4), and kept at −80°C before use. These proteins were characterized by western blotting analysis (Fig. S1A).

Peptide solution preparation

The synthesized peptide solution was prepared freshly before use as follows. Stock solutions of RADA and mRADA (1 v/v%) were diluted to 0.5 v/v% with autoclaved distilled water. Stock solutions of Ncad-mRADA and Ncad-Fc, which both contain 80 ng/μl N-cadherin, were diluted 50% by adding 1 v/v% mRADA stock solution. These peptide solutions were adjusted to neutral pH before use by PBS. We named the hydrogel formed from the mixture of Ncad-mRADA and mRADA peptide solution as "Ncad-mRADA hydrogel", and that from the mRADA peptide solution containing Ncad-Fc protein as "Ncad hydrogel". Selenomethionine-labeled mRADA stock solution (1 v/v%) was either diluted with autoclaved distilled water or with Ncad-mRADA stock solution to make 0.5 v/v% solutions.

Incorporation and release assay

Incorporation of EGFP, EGFP-mRADA, Ncad-Fc and Ncad-mRADA into the mRADA hydrogels was evaluated as follows. Fifty microliters of 2% mRADA solution at pH 3 was mixed with 50 μL of EGFP, EGFP-mRADA, Ncad-Fc or Ncad-mRADA (50 ng) in PB (pH 7.4). After incubation at 37°C in a CO_2 incubator for 24 hours (h), the hydrogels were washed with 250 μL phosphate buffered saline (PBS) (pH 7.4). The

concentration of EGFP and EGFP-mRADA in the soluble fraction was measured by ELISA. EGFP and EGFP-mRADA incorporation were calculated using the following formula. Protein incorporation (%) = [(weight of input) – (weight of the soluble fraction)] / (weight of input) × 100 (%). mRADA hydrogels incorporated with EGFP-mRADA as described above were washed with PBS three times and incubated with 200 μL 10% FBS in PBS at 37°C and at 500 rpm (CM-1000; EYELA, Tokyo, Japan). After 6, 12, 24, 72, 96, 168, and 336 h, the soluble fractions were collected and then incubated with 200 μL 10% FBS in PBS. EGFP-mRADA release was calculated using the following formula. Unreleased protein / incorporated protein (%) = [(weight of incorporated protein) – (total weight of the soluble fraction)] / (weight of incorporated protein) × 100 (%). Incorporation and sustained-release assays were performed two times independently and evaluated. The incorporation and release of Ncad-Fc and Ncad-mRADA were evaluated by western blot analysis. The soluble fraction samples after incorporation, PBS-washing, and 144 h-incubation were concentrated using an ultrafiltration column (Amicon Ultra 10K, Merck). The collected samples were mixed with sodium dodecyl sulfate loading buffer and analyzed by sodium dodecyl sulfate-polyacrylamide gel electrophoresis on 7.5% polyacrylamide gels. The proteins were then electroblotted onto polyvinylidene fluoride membranes using an iBlot Gel Transfer Device (Thermo Fisher Scientific). The membranes were blocked with 5% skimmed milk for 1 h at room temperature, incubated with a rabbit anti-N-cadherin antibody (1:5,000, ab76011; Abcam) for 16 h at 4°C, and then incubated with a peroxidase-labeled goat anti-rabbit IgG (1:5,000, Dako, Glostrup, Denmark) for 2 h. The bands were detected using SuperSignal West Femto Maximum Sensitivity Substrate (Thermo Fisher Scientific) and visualized using a Sayaca-Imager (DRC; Tokyo, Japan).

V-SVZ-derived neuroblast culture

Glass-bottom 35-mm Petri dishes coated with the mRADA, Ncad, or Ncad-mRADA hydrogels were prepared prior to cell preparation. The dishes were incubated with the biomaterial solution for 30 min at 4ºC and for a further 30 min at 37ºC. The dishes were rinsed once with PBS (pH 7.4) and air-dried in a laminar flow hood until use.

V-SVZ tissues were dissected from postnatal day 0 (P0)–P1 ICR mice. Pooled tissues were dissociated with trypsin-EDTA (Thermo Fisher Scientific). The cells were washed with L-15 medium (Thermo Fisher Scientific) containing 20 μg/ml DNaseI (Roche). The cell aggregates were embedded in 50% Matrigel (BD Biosciences) and diluted in Hank's balanced salt solution (Thermo Fisher Scientific). The cells were cultured in Neurobasal medium containing 2% B-27 supplement, 2 mM L-glutamine and

50 U/ml penicillin-streptomycin at 37ºC with 5% CO_2 for 48 h before imaging. Details of the cell preparation are described elsewhere [33].

Time-lapse video recordings were performed using a BZ-X800 fluorescence microscope (Keyence, Osaka, Japan) equipped with a ×20 dry objective lens. Images were obtained every 1 or 5 min for 24 h under humidified conditions at 37ºC with 5% CO_2. The migrating neuroblasts identified by their small mono/bipolar morphology and saltatory movement were analyzed using a manual tracking plugin of the ImageJ software (National Institutes of Health, Bethesda, MD, USA). The resting phase was defined as a migration speed slower than 0.1 μm/min.

Ischemic stroke

Cerebral stroke was induced in 12–16-week-old male mice. Mice were deeply anesthetized by spontaneous inhalation of 1–2% isoflurane in oxygen and placed on a 37°C heated bed (model BMT-100, Bio Research Center, Nagoya, Japan). Middle cerebral artery occlusion (MCAO) was induced by the intraluminal filament technique, as reported previously [34] with several modifications. In brief, after occlusion of the common carotid artery, the right carotid bifurcation was exposed, and the external carotid artery was coagulated distal to the bifurcation. A 10.0-mm silicone-coated 8-0 filament was then inserted through the stump of the external cerebral artery and gently advanced to occlude the middle cerebral artery, and the incision was closed. The mice were re-anesthetized 40 min later, the incision was re-opened, and the filament was gently withdrawn. The incision was then closed again. After this procedure, mice were returned to their home cage. Since the extent of stroke-induced neuroblast migration is strongly correlated with the infarct size, we only used individuals with strong GFAP signal covering 10-25% of the ipsilateral hemisphere for analysis of post-MCAO samples.

The animals were ranked according to their body weight loss during the first one week after MCAO, and then successively assigned to treatment groups so that the mean body weight loss in each group was about the same.

In sham operation, under deep anesthesia, right common carotid artery was exposed, but not occluded, and then the incision was closed.

Cryogenic brain injury

Cortical cryogenic injury was performed on postnatal day 2 (P2) mice or 10–16-week-old male mice as described previously [16,21]. Mice were placed in a stereotaxic instrument (David Kopf Instruments, US) and anesthetized with 1% isoflurane in oxygen (0.3 L/min) and the skull was exposed through a scalp incision. A pre-chilled hexagonal wrench was prepared in liquid nitrogen; a 1.2 mm-wide and a 3.0 mm-wide wrench for

neonatal and adult mice, respectively. The metal probe was placed on the exposed right skull (0.5-mm anterior and 1.2-mm lateral to lambda for P2 mice and 0.5-mm anterior and 1.2-mm lateral to bregma for adult mice) for 10 seconds. For neonatal mice, the procedure was repeated three times with a time interval of 5 seconds to re-chill the probe, while the procedure was repeated 12 times for adult mice. The scalp was sutured and the mice were placed in a heated recovery box for 15 min, and then returned to their home cage.

Injection of self-assembling peptides

Mice were deeply anesthetized by spontaneous inhalation of 1–3% isoflurane. Prior to injection of the self-assembling peptides, the scalp and parietal bone near the injection sites were resected to expose the brain. The peptide solution was loaded into a glass capillary needle and slowly stereotaxically injected into either intact or injured brains as follows. Adult 8–10-week-old male mice were used for intact mice injection experiments. 2.5 µl of the peptide solution was injected into the right and left medial striata (coordinates: 1.3 mm anterior, 1.3 mm lateral to bregma, 2.0–2.6 mm deep). Injection of 3 µl peptide solution throughout the striatum from the lateral wall of the lateral ventricle of intact adult or 13±1 day-post-MCAO mice was performed by tilting the head to an angle of 45° (coordinates: 1.55 mm anterior, 0.8 mm lateral to bregma, 1.5–3.0 mm deep). Intracortical injection was performed on 2-day-post-cryoinjured mice and 2.5 µl peptide solution was slowly injected into the lesion site (coordinates: 0.5 mm anterior, 0.95 mm lateral to bregma, 1.4–2.2 mm deep from the skull surface). Neonatal 4-day-post-cryoinjured mice were subjected to intracortical injection of 2 µl peptide solution into the lesion site (1.0–1.5 mm deep from the skull surface). After the injection, the capillary needle was kept in the injection site for 5–7 min, until hydrogel formation was accomplished. Mice were transcardially perfused 5 or 25 days after the injection with PBS (pH 7.4), followed by 4% paraformaldehyde (PFA) in 0.1 M PB (pH 7.4). Tissues were further fixed in the same fixative overnight.

Postnatal V-SVZ electroporation

Neonatal ICR or *NSE-DTA* pups (P0–1) were anesthetized by hypothermia (1 min) and fixed in a stereotaxic instrument. A pulled glass capillary needle was loaded with 2 µl plasmid solution (4 µg/ml *pCAGGS-EmGFP* [35] in distilled water containing 0.01% Fast Green). The capillary needle was placed into the lateral ventricle of the right hemisphere (2.0 mm anterior, 1.2 mm lateral to lambda and 2.0 mm deep) and the plasmid was injected. The animals were subjected to three electrical pulses (70 V, 20.0 msec) using a Super Electroporator NEPA21 Type II (Nepa Gene, Chiba, Japan) and 10 mm

tweezer electrodes (CUY650P10, Nepa Gene, Chiba, Japan). Electroporated animals were placed on a heating plate before being returned to their home cage.

Immunohistochemistry

Brain sections were prepared and stained as previously described [13]. Briefly, 50 or 60-μm-thick coronal sections were prepared with a vibratome VT1200S (Leica, Wetzlar, Germany). The sections were incubated in blocking solution (10% normal donkey serum, 0.4% Triton X-100 in PBS) for 60 min at room temperature, then in primary antibody solution overnight at 4°C, followed by secondary antibody solution containing AlexaFluor-conjugated secondary antibodies (1:1,000, Thermo Fisher Scientific) for 2 h at room temperature. Signals were amplified with biotinylated secondary antibodies (1:500, Jackson Laboratory, West Grove, PA, USA) and the Vectastain Elite ABC kit (Vector Laboratories, Burlingame, CA, USA), and visualized using the TSA Fluorescence System (Akoya Biosciences, Marlborough, MA, USA). The Click reaction was used to visualize the alkyne-modified RADA and mRADA hydrogels by incubating sections in Click reaction solution [100 mM Tris-HCl (pH 8.0), 15 mM $CuSO_4$, 0.5 mM Tris (3-hydroxypropyltriazolylmethyl) amine (Tokyo Chemical Industry Co., Ltd.), 200 mM ascorbic acid, AlexaFluor 647-conjugated azide (Alexa647-azide, 1:50, Thermo Fisher Scientific)] for 30 min at room temperature. For CD31 staining, sections were pretreated with 1% H_2O_2 for 40 min before blocking. The following primary antibodies were used: goat anti-Iba1 (1:1,000, Abcam), rabbit anti-Iba1 (1:2,000, Wako Pure Chemical Industries, Osaka, Japan), guinea-pig anti-DCX (1:800, Millipore), rabbit anti-DCX (1:500, Cell Signaling Technologies), mouse anti-S100β (1:200, Sigma-Aldrich, St. Louis, MO, USA), rabbit anti-GFAP (1:1,000, DAKO), chicken anti-GFAP (1:10,000, Abcam), rat anti-CD31 (1:100, BD Biosciences), rat anti-GFP (1:500, Nacalai, Kyoto, Japan), rabbit anti-GFP (1:500, MBL, Tokyo, Japan), mouse anti-MAP2 (1:500, Sigma Aldrich), rabbit anti-GAD67 (1:500, Millipore), mouse anti-Gephyrin (1:1,000, Synaptic Systems), rabbit anti-NeuN (1:1,000, Abcam), and mouse anti-NeuN (1:200, Millipore). Cell nuclei were stained with Hoechst 33342 stain (1:5,000, Invitrogen). For quantification, coronal sections including the V-SVZ were used. To visualize the area positive for immunostaining and to count cells, confocal z-stack images were captured using an LSM700 confocal laser microscope (Carl Zeiss, Jena, TH, Germany) equipped with 10×/0.45, 20×/0.8 and 40×/1.2 objective lenses, or an Olympus FV3000 confocal microscope (Evident, Tokyo, Japan) equipped with 10×/0.4, 20×/0.8 and 40×/1.4 objective lenses. To measure GFAP+ area, z-stack images were captured using a BZ-X810 fluorescence microscope (Keyence, Osaka, Japan) with a 20×/0.75 objective lens. ImageJ (National Institutes of Health, Bethesda, MD, USA), Zen (Carl Zeiss, Jena,

Germany) and cellSens (Evident, Tokyo, Japan) were used for measurement. The images of spines and neurites were captured using LSM880 confocal laser microscope (Carl Zeiss, Jena, TH, Germany) equipped with Airyscan FAST (Carl Zeiss) in super-resolution mode with a water-immersion 40×/1.2 (zoom 1.8) or oil-immersion 63×/1.4 (zoom 3.0) objective lens. The gamma value was adjusted by Imaris (Bitplane, Oxford, United Kingdom) to obtain images (Fig. 2C", D").

Histological analyses

Histological analyses of coronal sections were performed as follows. For the analysis of Iba1+ microglial cells in the intact adult brain, sections were immunostained for Iba1 and the hydrogel was visualized with Alexa647-azide. A single section containing hydrogel in the striatum was selected from each animal. The Iba1+ area was analyzed using ImageJ (National Institutes of Health, Bethesda, MD, USA). For analysis of Dcx+ neuroblasts in the intact adult brain, sections containing hydrogel were selected. The number of Dcx+ cells in every third section was counted and the number multiplied by three to obtain the total number of Dcx+ cells per brain.

The number of Dcx+ neuroblasts in the ipsilateral striatum of post-MCAO samples was obtained from sequential sections containing the hydrogels. To quantitatively analyze GFAP and CD31 expression in MCAO brains, sections were imaged for GFAP+ or CD31+ cells and the area within 100 μm from the injection site was analyzed. The area within 100 μm from the V-SVZ was excluded from the analysis.

Dcx+ neuroblasts in the cortex were quantified in adult cryoinjured brain slices. To visualize and quantitatively analyze Dcx+ cells, confocal z-stack images were captured. The sections with injected hydrogels on the dorsal wall of the lateral ventricle were selected for further analysis. The number of Dcx+ neuroblasts in every sixth section was counted and the neuroblast number was multiplied by six to obtain the total number of cells per brain.

Dcx+ neuroblasts were quantified in neonatal cryoinjured brain slices. To visualize and quantitatively analyze Dcx+ cells in and around the hydrogels, confocal z-stack images with a step size of 2 μm were captured. The number of Dcx+ cells in every sixth section was counted and the hydrogel or lesion site area was measured to obtain the density of Dcx+ cells.

The number of regenerated neurons in ICR mice was counted in all coronal sections containing the injection and lesion track. The sections were co-stained for NeuN and GFP to visualize mature neurons and V-SVZ-derived cells. The number of NeuN+GFP+ co-expressing cells was counted from every second coronal sections for *NSE-DTA* mice experiments and the cell number was multiplied by two to obtain the total

number of cells per brain. The numbers of NeuN- and GFP-immunoreactive cells were counted under an optical microscope (Olympus BX-51, Evident, Tokyo, Japan) with a 20× objective lens.

Transmission electron microscopy

Adult wild-type mice five days after RADA or mRADA injection and cryoinjured neonatal *Dcx-EGFP* mice four days after selenomethionine-labeled Ncad-mRADA injection were fixed at P9 by transcardiac perfusion with 2% PFA and 2.5% glutaraldehyde containing 0.1 M PB. The brain was extracted and post-fixed for 48 h in the same fixative at 4ºC and sliced into 200 μm coronal sections using a vibratome (VT1200S, Leica). Appropriate sections, including the center of injury, injected biomaterials, and migrating neuroblasts in the neocortex were selected for further processing from cryoinjured brains based on images of EGFP fluorescence. The selected sections were treated with 4% OsO_4 in 0.1 M PB for 90 min, dehydrated in graded concentrations of ethanol and propylene oxide and embedded in epoxy resin (Durcupan, Sigma Aldrich) for 72 h in a 60ºC oven to complete polymerization of the resin. Serial semi-thin sections (1.5-μm-thick) were cut with an ultramicrotome (UC7, Leica) using a diamond knife (Histo, Diatome, Hatfield, PA, USA), and stained lightly with 1% toluidine blue. After acquisition of the images with a transmitted light microscope (Olympus BX51, Evident, Tokyo, Japan), the semi-thin sections were glued to Durcupan blocks and detached from the glass slide by repeated freezing in liquid nitrogen and thawing. Ultra-thin sections (60–70-nm-thick) were prepared from the semi-thin sections using an ultramicrotome (UC7, Leica) and a diamond knife (SYM2045, Syntek, Kanagawa, Japan), and stained with 2% uranyl acetate for 15 min and with modified Sato's lead solution (Reynolds' solution) for 5 min. Images were captured using a transmission electron microscope (JEM-1400Plus, JEOL, Tokyo, Japan) equipped with a digital camera.

Deletion of V-SVZ-derived cells differentiating into neuronal lineage cells

P0 *NSE-DTA* mice [29,36] or C57BL/6J mice were anesthetized by brief hypothermia and electroporated with the EmGFP encoding plasmid as described above. On the next day (at P1), 1 μl solution of adenovirus encoding Cre recombinase under the control of the cytomegalovirus promoter Ad-CMV-iCre (Vector Biolabs, Cat. 1045) was stereotaxically injected into the right lateral ventricle (2.0 mm anterior, 1.2 mm lateral to lambda and 2.0 mm deep). These mice were subjected to cryogenic cortical injury at P2, followed by Ncad-mRADA injection into the injured sites at P5. Histological analyses were performed using brain tissues fixed at P30 after the foot-fault test (see below).

Neurological assessments

Mice were subjected to quantitative neurological testing from P29-35. The body weight was not statistically different among experimental groups.

Foot-fault test: The foot-fault test was performed on cryo-injured mice as previously described with modifications [37]. Briefly, mice roamed on 20-cm elevated hexagonal wire grids with 40-mm diameter openings for 10 min on a day prior to the test. During the test, each mouse was tested for 5 min on the grid and the total number of steps and foot-faults for the left hindlimb were recorded. A misplaced limb that slipped on the grid or fell through the openings in the grid was counted as a foot-fault. The number of foot-faults for the left hindlimb was divided by the total number of hindlimb steps to determine percentage of the fault steps. The test was repeated twice on the same day for each mouse and the fault rate averaged.

Automatic gait analysis: Gait analysis was performed using the Noldus CatWalk XT (Noldus Information Technology, Wageningen, the Netherlands), an automated gait analysis system, according to the manufacturer's instructions. Briefly, in a dark environment, the mice were allowed to walk across a glass walkway illuminated with a green light that was completely reflected internally except at the points receiving pressure. The contact point of each paw on the glass was illuminated, which was recorded with a high-speed video camera. The footprints recorded during each trial were analyzed using the CatWalk XT 10.5 software to generate a series of parameters. At least three successful sustained walk recordings for each mouse were used for each analysis, and the average of the runs was reported. Among the multiple parameters, maximum contact area, the paw area at the moment of maximum floor contact with the plate during a stance phase, was compared among the experimental groups, as reported previously [16]. Since the paw contact area was strongly correlated with the body weight, only the mice with average body weight (mean ± 2-fold standard deviation) were used for this experiment.

Statistical analysis

All data were analyzed using BellCurve for Excel (SSRI, Japan) and GraphPad Prism 9 (GraphPad Software, USA). At least three independent experiments were performed for each analysis. Data are expressed as the mean ± standard error of the mean (SEM) or as box and whisker plots with individual data points (in detail: median, upper box bound (75%), lower box bound (25%), minus whisker, plus whisker). The Shapiro-Wilk test (p value <0.01) or Bartlett's test (p value <0.01) and the F-test (p value <0.01) were performed prior to the following tests. Comparisons between two groups were performed with Student's t-test, Welch's t-test or the Wilcoxon rank sum test. When three

or more groups were compared, we applied the one-way ANOVA followed by the Bonferroni post hoc test or the Kruskal-Wallis test followed by the Steel-Dwass test. The one-way ANOVA test with a two-stage step-up method of Benjamini, Krieger and Yekutieli [38,39] was used to correct for multiple comparisons by controlling the False Discovery Rate in the behavioral tests. A p value < 0.05 and a q value < 0.05 were considered statistically significant.

Results

Ncad-mRADA stably incorporates in mRADA supramolecular hydrogel

We previously developed mRADA, which has reduced viscoelasticity compared with the original RADA [27]; however, the interaction of mRADA with the surrounding tissue after injection into the brain has not been investigated. Among the previously reported glycine substitution form of the RADA peptides, [(RADG)-$(RADA)_3$] also showed lower viscoelasticity as mRADA [$(RADA)_3$-(RADG)]. In this study, we used mRADA because [(RADG)-$(RADA)_3$] formed relatively shorter and fragmented fibrils, mostly with 100-nm lengths, than mRADA that formed well-developed μm-long nanofibers, which are expected to incorporate peptide-tagged protein more effectively. We injected self-assembling mRADA and RADA peptides into the striatum of adult mice, and then fixed five days later. The brains were sliced, and embedded into resin to prepare semi-thin (1.5 μm-thick) sections. Staining of sections with toluidine blue and light microcopy observation revealed that RADA formed large aggregates sharply demarcated from the parenchyma, in which only a few cells were observed (Fig. 1A–A”). In contrast, the boundary between the brain parenchyma and the mRADA hydrogel was irregular and unclear, and many cells were distributed in these areas (Fig. 1B–B”). We then investigated the precise distribution of the hydrogels in brain parenchyma using transmission electron microscopy. While RADA hydrogel was only observed along the injection scars (Fig. 1C–C’), thin aggregates of mRADA hydrogel with various morphologies were widely distributed in and around the injection scars (Fig. 1D–D’). Some of the mRADA fibers were connected with blood vessels or resident neurons or glial cells, indicating that a single injection of mRADA peptides can provide a scaffold for cell migration to a wide area of the brain.

We recently found that RADA-tagged EGFP (EGFP-RADA) was efficiently incorporated into RADA hydrogels and more than 90% of the incorporated EGFP-RADA remained in the RADA hydrogel after 168 h [30]. Here, we generated mRADA-tagged EGFP (EGFP-mRADA) and examined its incorporation and release from mRADA hydrogel. As expected, there was a difference in incorporation efficiency between EGFP-mRADA and non-tagged EGFP: EGFP-mRADA was incorporated at 66 mol%, while the incorporation of non-tagged EGFP was limited to 17 mol% (Fig. 1E). In a time-course EGFP release assay, 96 mol% of EGFP-mRADA remained in mRADA hydrogel after incubation for 336 h (Fig. 1F).

Using the mRADA expressing plasmid, we constructed a plasmid vector encoding mRADA tagged with N-cadherin extracellular domain. HEK293T cells were transfected with the plasmids to obtain Ncad-mRADA protein. In the presence of an excess amount

of mRADA peptides and in physiological pH and ionic conditions, such as those in brain tissue and used in tissue culture, the Ncad-mRADA protein self-assembled and formed an Ncad-mRADA supramolecular hydrogel (Fig. 1G). The rheological measurement analysis indicated that Ncad-incorporation into the mRADA did not influence the hydrogelation property of mRADA (Fig. S1B-C). As with EGFP-mRADA, Ncad-mRADA was efficiently incorporated into an mRADA hydrogel and remained after incubation for 144 h (Fig. 1H). In contrast, although Ncad-Fc (Fc-tagged Ncad) was efficiently incorporated into mRADA hydrogel, Ncad-Fc was released when incubated for 144 h (Fig. 1I). These results indicate that Ncad-mRADA was stably assembled with mRADA hydrogel, while Ncad-Fc was not.

We have previously reported that an Ncad-Fc-conjugated gelatin sponge-like biomaterial promotes neuroblast migration into the injured neocortex of neonatal mice [16]. However, the sponge could not be transplanted beyond the corpus callosum (hereinafter referred to as the CC) into deeper areas of the brain such as the striatum. In contrast, the RADA, mRADA and Ncad-mRADA peptide solutions could be easily injected into the striatum. In addition, the Ncad-mRADA peptide solution injected into the adult mouse striatum formed loose hydrogel aggregates that intermingled well with the surrounding tissue, similarly to mRADA (data not shown). To evaluate the immunological response to these hydrogels, brain sections were immunostained for Iba1 (a marker for microglia) five days after injection of RADA, mRADA, or Ncad-mRADA solution into the striatum (Fig. 1J). The hydrogel aggregates were visualized by a chemical reaction with Alexa647-azide. Activated microglia with swollen ramified or amoeboid-like cell bodies were accumulated close to, but not within, the hydrogel aggregates. The percentage of Iba1+ area within 300 μm of the hydrogel in the striatum was not significantly different among the groups (Fig. 1K). Microglia in other brain regions did not show activated morphology. These observations indicate that Ncad-mRADA hydrogel disperses into the parenchyma and forms a histocompatible hydrogel with a high cellular affinity comparable to mRADA, and with a focal and limited immune response at the same level as that of RADA and mRADA.

Ncad-mRADA induces ectopic migration of neuroblasts

To analyze the ability of Ncad-mRADA hydrogel to act as a scaffold to support migration of V-SVZ neuroblasts *in vivo*, the self-assembling peptides or PBS were injected at an angle of 45 degrees to the cortex through the striatum to the V-SVZ (Fig. S2A). Five days later, the coronal brain sections were prepared and immunostained for Dcx (a marker for neuroblasts) (Fig. S2B). In the PBS group, almost all V-SVZ-derived neuroblasts migrated toward the olfactory bulb, not the striatum (data not shown), as is

seen under normal physiological conditions [40]. In contrast, neuroblasts were observed along the Ncad-mRADA hydrogel formed in the striatum (Fig. S2B). The numbers of Dcx+ neuroblasts distributed that were closer than 300 μm of the injection track were counted. The number of neuroblasts along the material in the striatum was significantly higher in the Ncad-mRADA group compared with that in the RADA or mRADA groups (Fig. S2C), indicating that the Ncad-mRADA hydrogel provided an efficient scaffold for neuroblasts to ectopically migrate into the brain parenchyma.

Ncad-mRADA promotes neuroblast migration towards injured adult striatum

After stroke, neuroblasts produced in the V-SVZ migrate toward the damaged area [12,41,42]. We examined whether Ncad-mRADA hydrogel promotes the post-stroke neuroblast migration using mice subjected to transient MCAO, which mainly produces infarcts in the lateral striatum. Since stroke-induced neuroblast migration is strongly correlated with the infarct size, we used only animals with moderate infarction (about 10-25% of the area of a hemisphere), which weakly induces neuroblast migration from the V-SVZ without interventions. Thirteen days after MCAO, the mice were injected with mRADA or Ncad-mRADA peptides or PBS from the V-SVZ to the lateral striatum at a 45° angle (Fig 2A–B). Five days later, coronal brain sections were prepared and immunostained for Dcx (Fig. 2C–D"), GFAP (a marker for astrocytes) (Fig. 2I, J), CD31 (a marker for vascular endothelial cells) (Fig. 2K, L) or Iba1 (Fig. 2M, N). We counted the number of neuroblasts in the V-SVZ (Fig. 2E), and in the striatum that were closer than 300 μm to the injection trajectory (Fig. 2F). There was no significant difference in the number of neuroblasts in the V-SVZ between the two groups (Fig. 2E). In the PBS treated group, very few neuroblasts were observed in the post-stroke striatum along the injection trajectory. mRADA injection slightly but significantly increased the number of Dcx+ neuroblasts individually distributed along the hydrogel compared with the PBS group (Fig. 2C, C', C"). In contrast, much more neuroblasts were distributed in and around the Ncad-mRADA hydrogel, some of which formed chain-like clusters (Fig. 2D, D', D"). The number of neuroblasts in the post-stroke striatum was significantly higher in the Ncad-mRADA group compared with that in the mRADA group or PBS group at all distances from the V-SVZ analyzed (Fig 2F). The majority of these neuroblasts were distributed inside or near (< 200 μm) the Ncad-mRADA scaffold (Fig. 2F).

Astrocytes and blood vessels were also observed in and around the biomaterials in both groups at 18 days after MCAO (Fig. 2I–L). A comparison of their distribution in the area within 100 μm from the injection trajectory showed that the GFAP+ area percentage and the total CD31+ vessel length were not significantly different between the groups (Fig. 2G–H). Microglia were accumulated around but did not intrude into the hydrogel

areas (Fig 2M–N). We also compared the effects of biomaterial injection on immune cell infiltration by immunohistochemistry of a leukocyte common antigen CD45. The density of leukocytes strongly expressing CD45 ($CD45^{high}$ cells) around the hydrogel was not significantly different between the mRADA and Ncad-mRADA groups (Fig. S4).

We examined whether the V-SVZ-derived neuroblasts migrating along the biomaterials could mature into neurons in the injured striatum using genetic labeling of neural stem cells and their progeny. In Nestin-CreER;R26R-ECFP mice [43,44], tamoxifen administration induces nuclear transfer of Cre recombinase in nestin promoter active neural stem/progenitor cells, which results in removal of a "floxed" STOP sequence at the Rosa 26 locus, leading to persistent expression of a fluorescent protein ECFP. After tamoxifen injection (100 mg/kg/day, once a day for two days), these mice were subjected to MCAO and biomaterial injection, and then fixed at 56 days. We found some of the ECFP-labeled cells distributed along the needle tracks expressing mature neuronal marker NeuN, but not Dcx (Fig. S3B-C). The number of these cells was significantly higher in the Ncad-mRADA group compared with that in the mRADA group (Fig. S3D), suggesting that Ncad-mRADA treatment increased generation of mature neurons derived from V-SVZ neural stem/progenitor cells in the injured striatum. We performed the foot-fault test, a behavior test for sensorimotor function, in these mice before and after the biomaterial injection. While the intact animals show about 50% of the ratio of left foot fault, the animals 12 days after right MCAO (one day before biomaterial injection) increased this value to about 70% in both of the groups, reflecting their sensorimotor disfunction at the contralateral limbs. The value tended to become lower in Ncad-mRARA group than mRADA group, but failed to reach statistical significance (Fig. S3E-G).

Taken together, these results indicate that Ncad-mRADA efficiently promotes migration of Dcx+ neuroblasts toward the injured striatum in an N-cadherin-dependent manner, leading to increase in mature new neurons in the post-stroke brain.

Ncad-mRADA promotes neuroblast migration towards injured adult neocortex

We investigated whether Ncad-mRADA promotes neuroblast migration toward the neocortex after focal lesion. Two days after a cryogenic lesion was made in the parietal neocortex, the self-assembling peptides were injected from the V-SVZ to the cortical surface through the injured area, and brain sections were prepared five days later (Fig. 2O–P). Many neuroblasts were found in and around the Ncad-mRADA scaffold, but few were seen in the mRADA scaffold (Fig. 2Q–R"). The number of neuroblasts in the neocortex was significantly higher in the Ncad-mRADA group in areas 300 μm or more

from the V-SVZ (Fig. 2T). There was no significant difference in the number of neuroblasts in the V-SVZ (Fig. 2S).

These results indicate that appropriately implanted Ncad-mRADA scaffolds can promote migration of neuroblasts to injured areas in the striatum and neocortex, without affecting neuroblast production in the V-SVZ.

mRADA containing N-cadherin provides an efficient scaffold for neuroblast migration *in vitro*

To precisely investigate the effect of Ncad-mRADA on neuroblast migration, we performed time-lapse imaging of V-SVZ neuroblasts on culture dishes coated with mRADA or Ncad-mRADA hydrogel (Fig. 3A–E). The speed of neuroblast migration was significantly higher on Ncad-mRADA compared with that on mRADA (Fig. 3A–B, Sup. Movie 1). The V-SVZ neuroblasts move in a saltatory manner, repeating migrating and resting phases [45]. The neuroblasts on Ncad-mRADA hydrogel migrated with a significantly longer stride (Fig. 3C), shorter saltatory cycle length (Fig. 3D), and shorter resting phase (Fig. 3E) compared with those on mRADA. We also examined whether mRADA mixed with immunoglobulin Fc domain-conjugated N-cadherin (Ncad hydrogel) in which N-cadherin indirectly interacts with mRADA, likely through the Fc domain, promotes neuroblast migration. There were no significant differences in migration parameters between the neuroblasts on Ncad-mRADA hydrogel and those on Ncad hydrogel (Fig.3B–E). Similar results were obtained in cultures using Dcx-EGFP mouse V-SVZ in which neuroblasts were identified by their GFP expression (Fig. S5). Therefore, in culture conditions, the promotion of neuroblast migration by N-cadherin did not depend on its stable association with the mRADA hydrogel.

Ncad-mRADA promotes neuroblast migration towards the injured neocortex in neonatal mice

We have previously reported that N-cadherin plays a key role in neuroblast migration along radial glial fibers in injured neonatal neocortex [16]. Therefore, we tested the effect of the Ncad-mRADA scaffold on neuroblast migration in injured neonatal cortex. Postnatal day 2 (P2) animals were subjected to cryogenic injury of the parietal cortex. The self-assembling peptides that form mRADA, Ncad-mRADA, or Ncad hydrogels were then injected into the injured area at P5, and brain sections processed at P9 (7 days post-injury). Dcx+ neuroblasts were abundant in the Ncad-mRADA hydrogels, but sparse in the mRADA and Ncad hydrogels (Fig. 3F). The density of Dcx+ cells in the injected areas was significantly higher in the Ncad-mRADA group compared with that in mRADA or Ncad groups (Fig. 3G), indicating that Ncad-mRADA hydrogel efficiently

promoted neuroblast migration toward the injured neocortex *in vivo*. These data also indicate that such *in vivo* effects of Ncad-mRADA depend on the stable association of N-cadherin with mRADA scaffolds.

The neuroblasts were widely distributed above the V-SVZ, i.e., from the corpus callosum to the injured cortical surface. We compared the density of neuroblasts in areas at different distances from the V-SVZ between the mRADA and Ncad-mRADA groups. In this analysis, the neocortex was divided into three areas: upper (superficial), middle and lower (deeper) (Fig. 3H–H'). The density of neuroblasts was significantly higher in the Ncad-mRADA group in the upper and middle layers, but not in the lower layer, CC, or V-SVZ, compared with those in the mRADA group (Fig. 3I). Taken together, these data indicate that Ncad-mRADA significantly promotes neuroblast migration toward the neocortex, resulting in their widespread distribution throughout the cortical layers.

Neuroblasts directly interact with the Ncad-mRADA scaffold to migrate into the injured neocortex

Using transmission electron microscopy, we closely observed the spatial interaction between neuroblasts and transplanted Ncad-mRADA hydrogel in the neocortex 7 days after cryogenic injury (Fig. 4A–H). As shown in Fig. 1D', Ncad-mRADA hydrogels were well intermingled with brain tissues. To facilitate observation of Ncad-mRADA hydrogel distribution in the injured brain, which contains much cell debris and many inflammatory cells, we constructed selenomethionine-labeled Ncad-mRADA. Under electron microscopy, the Ncad-mRADA hydrogel could be recognized as organelle-free areas filled with a meshwork of small fibrous structures in necrotic tissues where activated microglia containing many vacuoles and lysosomes were accumulated. As we previously reported, neuroblasts were identified by their smooth and elongated cell bodies, a small elongated nucleus with lax chromatin, and scant cytoplasm containing many free ribosomes and microtubules [46]. Interestingly, neuroblasts occasionally formed chain-like clusters (Fig. 4A–C), with small adherens junctions and free spaces between cells (Fig. 4D), which are common features of chain migrating neuroblasts [46]. The cell bodies of these neuroblasts directly contacted the small fibrous structures in the Ncad-mRADA hydrogel (Fig. 4E). In addition, some neuroblasts migrated individually along the Ncad-mRADA fibers showing radial glia-like elongated morphology (Fig. 4F–H). Taken together, these observations strongly indicate that Ncad-mRADA provided an efficient scaffold to help neuroblasts migrate in a chain and individually inside necrotic brain tissue.

Ncad-mRADA promotes neuronal regeneration and sensorimotor improvement after neocortical injury

Having shown that Ncad-mRADA implantation increased the number of neuroblasts in injured neocortex (Fig. 3F–I), we then tested whether they mature into neurons and contribute to neurological recovery. To label V-SVZ-derived cells, we injected plasmids encoding Emerald Green Fluorescent Protein (EmGFP) into the lateral ventricle of P0 mice, and introduced them into the periventricular cells using an electroporator. After cryogenic injury at P2 and scaffold injection at P5, expression of neuronal markers in the EmGFP-labeled cells were examined (Fig. 5A). At P9, some of the EmGFP cells in the corpus callosum and neocortex expressed Dcx, but not NeuN, regardless of the type of injected biomaterials (Fig. S6A-B). At P30, the damaged tissues were shrunk but were still distinguishable in coronal brain sections. The mRADA and Ncad-mRADA scaffolds were mostly disappeared by 4 weeks after injection (Fig 5B). We examined the distribution of V-SVZ-derived (EmGFP-labeled) cells that express the mature neuron marker NeuN in the injured area. Most of the EmGFP+NeuN+ cells were observed in the vicinity of the injury scars (Fig. 5B–C). These cells also expressed MAP2 (Fig. 5D), another marker for mature neurons, and GAD67, a marker for GABAergic neurons (Fig. 5E). These cells developed long and branched processes with many spines (Fig. 5C), a typical morphology of mature neurons. We found localization of inhibitory post-synaptic membrane protein Gephyrin in these spines (Fig. 5F), suggesting that these cells were mature functional neurons. The percentage of cortical EmGFP+NeuN+ cells distributed in the upper layer was significantly higher in the Ncad-mRADA group, compared with that in the mRADA group (Fig. 5G). Overall, the Ncad-mRADA scaffold helped neuroblast migration toward the lesion, which resulted in an increased number of new mature neurons in the upper layer of the neocortex, the most seriously damaged layer in this injury model.

The mice after neonatal cortical injury were subjected to three kinds of quantitative neurological assessments, the foot-fault test, automatic gait analysis and elevated body swing test at P29-35 (Fig. 5A). In the foot-fault test, we calculated the percentage of missteps (% error) in all steps of the hind limbs during the 5-min trial (Fig. 5H). The false rate was significantly increased in the group subjected to the cryogenic lesion without subsequent intervention. Mice with the Ncad-mRADA hydrogel, but not the mRADA hydrogel or non-histocompatible RADA hydrogel (Fig. 1A-A”), exhibited a significant decrease in the false rate, which was comparable to that in intact animals (Fig. 5H, S6E). In the automatic gait analysis, among various parameters automatically measured during free walking, we previously found that the maximum contact areas of the left fore and hind paws were significantly reduced in mice after right cortical injury [16]. Such injury-

induced alterations were cancelled in mice treated with Ncad-mRADA, but not mRADA (Fig. 5I-J). Elevated body swing test could efficiently detect asymmetric body movement in rodents. While intact animals swing their body to the left and right with almost the same rate, the neocortical injury significantly decreased the percentage of body swing to the right. Ncad-mRADA, but not mRADA hydrogel treatment significantly increased the ratio to the level comparable to that in the intact animals (Fig. S6C-D).

Finally, we examined whether the V-SVZ-derived new neurons were involved in sensorimotor improvement in mice injected with Ncad-mRADA peptide. We used NSE-DTA mice in which neuronal cells are selectively eliminated depending on Cre recombinase expression [29,36]. The NSE-DTA mice and wild-type mice were subjected to electroporation of EmGFP plasmid to label V-SVZ cells at P0, followed by injection of adenovirus encoding cre into the lateral ventricle at P1, cortical injury at P2, and Ncad-mRADA injection at P5 (Fig. 5K). At P30, the number of EmGFP-labeled (V-SVZ-derived) cells expressing NeuN was significantly smaller in NSE-DTA mice compared with that in wild-type mice (Fig. 5L). The percentage of left paw missteps in the foot-fault test was also significantly higher in the NSE-DTA group than wild-type group (Fig. 5M), suggesting that the V-SVZ-derived new neurons contributed to the Ncad-RADA peptide treatment induced improvement in sensorimotor function. Taken together, these results indicate that Ncad-mRADA efficiently promotes neuronal regeneration and recovery of sensorimotor function after neonatal brain injury.

Discussion

In this study, we developed Ncad-mRADA, an injectable biomaterial based on the structural and molecular features of radial glia, which forms an efficient migration scaffold for V-SVZ-derived neuroblasts in the postnatal brain. This scaffold successfully facilitated the migration of neuroblasts into deep and superficial lesions and promoted improvement in sensorimotor functions.

The mRADA hydrogel did not induce an excessive inflammatory response in the brain parenchyma (Fig. 1). Compared with the hydrogel formed by the original self-assembling peptide, RADA, the mRADA hydrogel showed greater ability to integrate into the surrounding tissue (Fig. 1) and to induce ectopic neuroblast migration to the striatum, which is distant from the V-SVZ (Fig. S2). Transmission electron microscopy revealed that mRADA hydrogel formed fine fibrous aggregates dispersed in parenchymal tissue (Fig. 1). The morphology of the mRADA hydrogel in tissue was in concordance with atomic molecular dynamics simulations that predicted fibrillar assembly with branched structures [27]. In addition, the highly fluid mRADA peptides could be

distributed more widely in the tissue surrounding the injection needle before aggregates formed compared with RADA peptides (Fig. 1A–D).

Notably, more than half of the ectopic neuroblasts were observed in regions ≥100 μm from the injection trajectory, where the Alexa647-azide signal was undetectable (Fig. S2). Considering that the Ncad-mRADA hydrogel showed a distribution profile similar to that of the mRADA hydrogel (data not shown), it is likely that these neuroblasts utilized the fine fibers of the Ncad-mRADA hydrogel that are not detectable with Alexa647-azide under light microscopy. Such a distribution profile is desirable for supplying neuroblasts throughout a lesion via a single injection (Fig. 2–3). Large aggregates of mRADA/Ncad-mRADA hydrogels labeled with Alexa647-azide were not detected by light microscopy at 4 weeks post-injection (Fig. 5), indicating that the hydrogels were degraded after the active period of tissue remodeling, a desirable feature of scaffold materials that promote tissue regeneration [1,47].

Radial glial cells are well-studied scaffold cells for neuroblasts in the embryonic brain. They extend a long process from the cell body, which is located in the ventricular zone, to the pial surface to serve as a scaffold for neuroblasts migrating into the neocortex during morphogenesis and after neonatal cortical injury. In both cases, the interaction between radial glia and migrating neuroblasts is mediated by N-cadherin [16,48]. Radial glial cells disappear within several weeks after birth [49]; therefore, neuroblasts use other scaffolds, such as blood vessels, and depend on β1 integrin-laminin signaling to reach injured areas in the adult brain [13]. Neuroblasts form chain-like elongated clusters to provide a scaffold for each other in the adult rostral migratory stream. N-cadherin is expressed in these adult-born neuroblasts [50] and in neuroblasts in the embryonic and neonatal brain, and is involved in neuroblast migration in the adult brain [51]. However, its application to the development of artificial scaffolds that mimic radial glial fibers has not been demonstrated. Here, we demonstrated that a biomaterial that forms radial glia-like fibers connecting the V-SVZ to a site of injury serves as an efficient scaffold that promotes neuroblast migration in an N-cadherin-dependent manner. The direct contact between neuroblasts and the biomaterial (Fig. 4) and the absence of astrocytes or blood vessels between them indicate that the preference for N-cadherin-containing scaffolds is maintained throughout life as a common feature of migrating neuroblasts.

Ncad-mRADA was constructed to stably and specifically associate the full-length N-cadherin extracellular domain tagged with mRADA to supramolecular nanofibers during mRADA self-assembly (Fig. 1G). The self-assembling mRADA forms a β-sheet structure in water through non-covalent interactions, such as hydrogen bonding and hydrophobic interactions. Given the capability of mRADA to form multivalent non-covalent interactions, it is likely that Ncad-mRADA assembles stably with mRADA

peptides. However, in “Ncad hydrogel” prepared by mixing Ncad-Fc with mRADA, the association of Ncad-Fc with the mRADA nanofibers was unstable because the association of Ncad-Fc depends on non-specific adsorption [30]. Both of these materials contained similar amounts of N-cadherin initially, but the Ncad hydrogel released the N-cadherin extracellular domain more rapidly during cell-free incubation (Fig. 1). After V-SVZ neuroblasts were cultured for 48 h, time-lapse imaging revealed that both Ncad-mRADA and Ncad hydrogels promoted neuroblast migration compared with the mRADA hydrogel (Fig. 3). However, histological analyses performed five days after injection into injured neocortex showed that neuroblast migration was promoted by Ncad-mRADA but not by Ncad hydrogel (Fig. 3). These results indicate that the stability of N-cadherin association is more important in tissue *in vivo* than in *in vitro* culture conditions. The persistence of neuroblast migration toward an injured area for at least one week [14], depending on the animal model, indicates that persistent N-cadherin activity might be critical for successful brain regeneration.

After termination of migration in the injured neocortex of neonatal mice, the V-SVZ-derived neuroblasts mature into neurons possessing long, branched neurites on which inhibitory synapses were formed (Fig. 5D-E). While the precise roles of these new neurons are still unknown, deletion of these new neurons using a genetic method cancels functional recovery in mice treated with Ncad-mRADA peptide (Fig. 5M). This indicates that the new neurons are involved in neuronal rewiring after injury. Considering the presence of extensive neuroblast migration into the neonatal human cortex [52], these data indicate that Ncad-mRADA fibers will be useful for the treatment of human neonatal brain injury. The Ncad-mRADA hydrogel also promoted neuroblast migration in the post-stroke adult brain (Fig. 2), and a small portion of these neuroblasts matured into NeuN+ neurons in the striatum (Fig. S3), but failed to cause statistically significant improvement in sensorimotor function (Fig. S3). In general, plasticity of neuronal circuits decreases with age [53]. Similarly, neurogenic activity in the V-SVZ is very high during the neonatal period but declines sharply within a month [54,55]. The decline in neurogenesis during postnatal development is more striking in primates, including humans [56–58]. Therefore, successful rewiring in adulthood requires more effective strategies that can maximize the utility of the limited number of newly born neurons. Self-assembling peptides containing a short functional peptide (for example, the RGD motif) that binds to integrins in the extracellular matrix promote axonal extension and neuroblast migration [26,59,60]. However full length protein domains also differentially mediate cell morphology, cell migration and cell proliferation compared with short peptide motifs alone [61]. Many proteins other than those that mediate cell adhesion cannot exert their functions with such a short sequence. Here, we have developed a technology for incorporating more than 100

kDa of full-length N-cadherin extracellular domain into the histocompatible self-assembling peptide, mRADA. This technique can be applied to incorporate other molecules with relatively large molecular sizes into injectable scaffolds. The scaffold-guided migration of neuroblasts in the injured brain depends on not only cell adhesion molecules but also diffusible factors such as BDNF released from the scaffolds [62]. Using a technique to release a diffusible factor from injectable nanofibers [30], in combination with the stable incorporation of cell adhesion molecules, it should be possible to design more effective biomaterials as migration scaffolds to continuously support neurogenesis until maturation in the injured brain.

Acknowledgements

The authors thank Mr. Jiro Nagase for technical support. The authors acknowledge the assistance of the Research Equipment Sharing Center at Nagoya City University. The authors also thank Sawamoto laboratory members for discussions and Jeremy Allen, PhD, from Edanz (https://jp.edanz.com/ac) for editing a draft of this manuscript.

Author contributions

Y Ohno: Formal analysis, Investigation, Validation, Visualization, Writing - original draft and editing. C Nakajima: Formal analysis, Investigation, Validation, Visualization, Writing - original draft and editing. I Ajioka: Resources, Formal analysis, Investigation, Validation, Visualization, Writing - original draft and editing. T Muraoka: Resources, Investigation, Validation, Visualization, Writing - original draft and editing. A Yaguchi: Resources. T Fujioka: Investigation. S Akimoto: Resources. M Matsuo: Investigation. A Lotfy: Investigation. S Nakamura: Formal analysis, Investigation. V Herranz-Pérez: Validation, Supervision. J M García-Verdugo: Validation, Supervision. N Matsukawa: Supervision. N Kaneko: Conceptualization, Formal analysis, Funding acquisition, Investigation, Supervision, Validation, Visualization, Writing - original draft, Writing - review and editing. K Sawamoto: Conceptualization, Funding acquisition, Project administration, Supervision, Writing - review and editing.

Funding

This work was supported by the Japan Agency for Medical Research and Development AMED [JP21bm0704033h0003 and JP21gm1210007 to K.S. and JP21jm0210060h0004 to N.K., I.A. and K.S.]; the Japan Society for the Promotion of Science (JSPS) KAKENHI [17H01392, 19H04757, 19H04785, 18KK0213, and 20H05700 to K.S. and 20H03565, 21H05106 to N.K.]; the Spanish Ministry of Science, Innovation and Universities [PCI2018–093062 to V.H-P. and J.M.G-V.]; the Spain Cell Therapy Network [TerCel-

RD16/0011/0026 to J.M.G-V.]; the JST FOREST Program (JPMJFR2146) to N.K. Bilateral Open Partnership Joint Research Projects [JPJSBP120229939 to N.K.]; Grant-in-Aid for Research at Nagoya City University [to N.K. and K.S.]; the Mitsubishi Foundation [to K.S.]; the Takeda Science Foundation [to N.K. and K.S.] and the Canon Foundation [to K.S. and I.A.].

Declaration of competing interest

The authors declare no competing interests.

Data availability

The data presented in this study are available on request from the corresponding authors.

References

[1] M.I. Echeverria Molina, K.G. Malollari, K. Komvopoulos, Design Challenges in Polymeric Scaffolds for Tissue Engineering, Front. Bioeng. Biotechnol. 9 (2021) 1–29. https://doi.org/10.3389/fbioe.2021.617141.

[2] T. Santos, C. Boto, C.M. Saraiva, L. Bernardino, L. Ferreira, Nanomedicine Approaches to Modulate Neural Stem Cells in Brain Repair, Trends Biotechnol. 34 (2016) 437–439. https://doi.org/10.1016/j.tibtech.2016.02.003.

[3] A. Cembran, K.F. Bruggeman, R.J. Williams, C.L. Parish, D.R. Nisbet, Biomimetic Materials and Their Utility in Modeling the 3-Dimensional Neural Environment, IScience. 23 (2020) 100788. https://doi.org/10.1016/j.isci.2019.100788.

[4] D. Carradori, J. Eyer, P. Saulnier, V. Préat, A. des Rieux, The therapeutic contribution of nanomedicine to treat neurodegenerative diseases via neural stem cell differentiation, Biomaterials. 123 (2017) 77–91. https://doi.org/10.1016/j.biomaterials.2017.01.032.

[5] K. Obernier, A. Alvarez-Buylla, Neural stem cells: origin, heterogeneity and regulation in the adult mammalian brain, Development. 146 (2019) dev156059. https://doi.org/10.1242/dev.156059.

[6] C. Nakajima, M. Sawada, K. Sawamoto, Postnatal neuronal migration in health and disease, Curr. Opin. Neurobiol. 66 (2021) 1–9. https://doi.org/10.1016/j.conb.2020.06.001.

[7] H. Wichterle, J.M. García-Verdugo, A. Alvarez-Buylla, Direct Evidence for Homotypic, Glia-Independent Neuronal Migration, Neuron. 18 (1997) 779–791. https://doi.org/10.1016/S0896-6273(00)80317-7.

[8] C. Lois, J.M. García-Verdugo, A. Alvarez-Buylla, Chain migration of neuronal precursors, Science (80-.). 271 (1996) 978–981. https://doi.org/10.1126/science.271.5251.978.

[9] P. Thored, A. Arvidsson, E. Cacci, H. Ahlenius, T. Kallur, V. Darsalia, C.T. Ekdahl, Z. Kokaia, O. Lindvall, Persistent Production of Neurons from Adult Brain Stem Cells During Recovery after Stroke, Stem Cells. 24 (2006) 739–747. https://doi.org/10.1634/stemcells.2005-0281.

[10] D. Alagappan, D.A. Lazzarino, R.J. Felling, M. Balan, S. V Kotenko, S.W. Levison, Brain Injury Expands the Numbers of Neural Stem Cells and Progenitors in the SVZ by Enhancing Their Responsiveness to EGF, ASN Neuro. 1 (2009) AN20090002. https://doi.org/10.1042/AN20090002.

[11] E. Llorens-Bobadilla, S. Zhao, A. Baser, G. Saiz-Castro, K. Zwadlo, A. Martin-Villalba, Single-Cell Transcriptomics Reveals a Population of Dormant Neural Stem Cells that Become Activated upon Brain Injury, Cell Stem Cell. 17 (2015) 329–340. https://doi.org/10.1016/j.stem.2015.07.002.

[12] T. Yamashita, M. Ninomiya, P.H. Acosta, J.M. García-Verdugo, T. Sunabori, M. Sakaguchi, K. Adachi, T. Kojima, Y. Hirota, T. Kawase, N. Araki, K. Abe, H. Okano, K. Sawamoto, Subventricular zone-derived neuroblasts migrate and differentiate into mature neurons in the post-stroke adult striatum, J. Neurosci. 26 (2006) 6627–6636. https://doi.org/10.1523/JNEUROSCI.0149-06.2006.

[13] T. Fujioka, N. Kaneko, I. Ajioka, K. Nakaguchi, T. Omata, H. Ohba, R. Fässler, J.M. García-Verdugo, K. Sekiguchi, N. Matsukawa, K. Sawamoto, β1 integrin signaling promotes neuronal migration along vascular scaffolds in the post-stroke brain, EBioMedicine. 16 (2017) 195–203. https://doi.org/10.1016/j.ebiom.2017.01.005.

[14] P. Thored, J. Wood, A. Arvidsson, J. Cammenga, Z. Kokaia, O. Lindvall, Long-term neuroblast migration along blood vessels in an area with transient angiogenesis and increased vascularization after stroke, Stroke. 38 (2007) 3032–3039. https://doi.org/10.1161/STROKEAHA.107.488445.

[15] M. Snapyan, M. Lemasson, M.S. Brill, M. Blais, M. Massouh, J. Ninkovic, C. Gravel, F. Berthod, M. Götz, P.A. Barker, A. Parent, A. Saghatelyan, Vasculature guides migrating neuronal precursors in the adult mammalian forebrain via brain-derived neurotrophic factor signaling, J. Neurosci. 29 (2009) 4172–4188. https://doi.org/10.1523/JNEUROSCI.4956-08.2009.

[16] H. Jinnou, M. Sawada, K. Kawase, N. Kaneko, V. Herranz-Pérez, T. Miyamoto, T. Kawaue, T. Miyata, Y. Tabata, T. Akaike, J.M. García-Verdugo, I. Ajioka, S. Saitoh, K. Sawamoto, Radial Glial Fibers Promote Neuronal Migration and

Functional Recovery after Neonatal Brain Injury, Cell Stem Cell. 22 (2018) 128-137.e9. https://doi.org/10.1016/j.stem.2017.11.005.

[17] N. Kaneko, V. Herranz-Pérez, T. Otsuka, H. Sano, N. Ohno, T. Omata, H.B. Nguyen, T.Q. Thai, A. Nambu, Y. Kawaguchi, J.M. García-Verdugo, K. Sawamoto, New neurons use Slit-Robo signaling to migrate through the glial meshwork and approach a lesion for functional regeneration, Sci. Adv. 4 (2018). https://doi.org/10.1126/sciadv.aav0618.

[18] N.S. Roy, C. Cleren, S.K. Singh, L. Yang, M.F. Beal, S.A. Goldman, Functional engraftment of human ES cell–derived dopaminergic neurons enriched by coculture with telomerase-immortalized midbrain astrocytes, Nat. Med. 12 (2006) 1259–1268. https://doi.org/10.1038/nm1495.

[19] T. Yamashita, H. Kawai, F. Tian, Y. Ohta, K. Abe, Tumorigenic Development of Induced Pluripotent Stem Cells in Ischemic Mouse Brain, Cell Transplant. 20 (2011) 883–892. https://doi.org/10.3727/096368910X539092.

[20] K. Ohnishi, K. Semi, T. Yamamoto, M. Shimizu, A. Tanaka, K. Mitsunaga, K. Okita, K. Osafune, Y. Arioka, T. Maeda, H. Soejima, H. Moriwaki, S. Yamanaka, K. Woltjen, Y. Yamada, Premature Termination of Reprogramming In Vivo Leads to Cancer Development through Altered Epigenetic Regulation, Cell. 156 (2014) 663–677. https://doi.org/10.1016/j.cell.2014.01.005.

[21] I. Ajioka, H. Jinnou, K. Okada, M. Sawada, S. Saitoh, K. Sawamoto, Enhancement of neuroblast migration into the injured cerebral cortex using laminin-containing porous sponge, Tissue Eng. - Part A. 21 (2015) 193–201. https://doi.org/10.1089/ten.tea.2014.0080.

[22] M.R. Caplan, P.N. Moore, S. Zhang, R.D. Kamm, D.A. Lauffenburger, Self-Assembly of a β-Sheet Protein Governed by Relief of Electrostatic Repulsion Relative to van der Waals Attraction, Biomacromolecules. 1 (2000) 627–631. https://doi.org/10.1021/bm005586w.

[23] G.A. Silva, C. Czeisler, K.L. Niece, E. Beniash, D.A. Harrington, J.A. Kessler, S.I. Stupp, Selective Differentiation of Neural Progenitor Cells by High-Epitope Density Nanofibers, Science (80-.). 303 (2004) 1352–1355. https://doi.org/10.1126/science.1093783.

[24] H. Yokoi, T. Kinoshita, S. Zhang, Dynamic reassembly of peptide RADA16 nanofiber scaffold, Proc. Natl. Acad. Sci. 102 (2005) 8414–8419. https://doi.org/10.1073/pnas.0407843102.

[25] S. Motamed, M.P. Del Borgo, K. Zhou, K. Kulkarni, P.J. Crack, T.D. Merson, M.I. Aguilar, D.I. Finkelstein, J.S. Forsythe, Migration and Differentiation of Neural Stem Cells Diverted From the Subventricular Zone by an Injectable Self-

Assembling β-Peptide Hydrogel, Front. Bioeng. Biotechnol. 7 (2019) 1–12. https://doi.org/10.3389/fbioe.2019.00315.
[26] R. Motalleb, E.J. Berns, P. Patel, J. Gold, S.I. Stupp, H.G. Kuhn, In vivo migration of endogenous brain progenitor cells guided by an injectable peptide amphiphile biomaterial, J. Tissue Eng. Regen. Med. 12 (2018) e2123–e2133. https://doi.org/10.1002/term.2644.
[27] A. Ishida, G. Watanabe, M. Oshikawa, I. Ajioka, T. Muraoka, Glycine Substitution Effects on the Supramolecular Morphology and Rigidity of Cell-Adhesive Amphiphilic Peptides, Chem. - A Eur. J. (2019). https://doi.org/10.1002/chem.201902083.
[28] S. Gong, C. Zheng, M.L. Doughty, K. Losos, N. Didkovsky, U.B. Schambra, N.J. Nowak, A. Joyner, G. Leblanc, M.E. Hatten, N. Heintz, A gene expression atlas of the central nervous system based on bacterial artificial chromosomes, Nature. 425 (2003) 917–925. https://doi.org/10.1038/nature02033.
[29] K. Kobayakawa, R. Kobayakawa, H. Matsumoto, Y. Oka, T. Imai, M. Ikawa, M. Okabe, T. Ikeda, S. Itohara, T. Kikusui, K. Mori, H. Sakano, Innate versus learned odour processing in the mouse olfactory bulb, Nature. 450 (2007) 503–508. https://doi.org/10.1038/nature06281.
[30] A. Yaguchi, M. Oshikawa, G. Watanabe, H. Hiramatsu, N. Uchida, C. Hara, N. Kaneko, K. Sawamoto, T. Muraoka, I. Ajioka, Efficient protein incorporation and release by a jigsaw-shaped self-assembling peptide hydrogel for injured brain regeneration, Nat. Commun. 2021 121. 12 (2021) 1–12. https://doi.org/10.1038/s41467-021-26896-3.
[31] M. Oshikawa, K. Okada, H. Tabata, K. Nagata, I. Ajioka, Dnmt1-dependent Chk1 pathway suppression is protective against neuron division, Development. 144 (2017) 3303–3314. https://doi.org/10.1242/dev.154013.
[32] X.-S. Yue, Y. Murakami, T. Tamai, M. Nagaoka, C.-S. Cho, Y. Ito, T. Akaike, A fusion protein N-cadherin-Fc as an artificial extracellular matrix surface for maintenance of stem cell features, Biomaterials. 31 (2010) 5287–5296. https://doi.org/10.1016/j.biomaterials.2010.03.035.
[33] M. Sawada, M. Matsumoto, K. Narita, N. Kumamoto, S. Ugawa, S. Takeda, K. Sawamoto, In vitro Time-lapse Imaging of Primary Cilium in Migrating Neuroblasts, Bio-Protocol. 10 (2020) 1–17. https://doi.org/10.21769/bioprotoc.3823.
[34] H. Hara, P.L. Huang, N. Panahian, M.C. Fishman, M.A. Moskowitz, Reduced Brain Edema and Infarction Volume in Mice Lacking the Neuronal Isoform of

Nitric Oxide Synthase after Transient MCA Occlusion, J. Cereb. Blood Flow Metab. 16 (1996) 605–611. https://doi.org/10.1097/00004647-199607000-00010.

[35] H. Ota, T. Hikita, M. Sawada, T. Nishioka, M. Matsumoto, M. Komura, A. Ohno, Y. Kamiya, T. Miyamoto, N. Asai, A. Enomoto, M. Takahashi, K. Kaibuchi, K. Sobue, K. Sawamoto, Speed control for neuronal migration in the postnatal brain by Gmip-mediated local inactivation of RhoA, Nat. Commun. 5 (2014) 4532. https://doi.org/10.1038/ncomms5532.

[36] I. Imayoshi, M. Sakamoto, T. Ohtsuka, K. Takao, T. Miyakawa, M. Yamaguchi, K. Mori, T. Ikeda, S. Itohara, R. Kageyama, Roles of continuous neurogenesis in the structural and functional integrity of the adult forebrain., Nat. Neurosci. 11 (2008) 1153–61. https://doi.org/10.1038/nn.2185.

[37] T.D. Hernandez, T. Schallert, Seizures and recovery from experimental brain damage, Exp. Neurol. 102 (1988) 318–324. https://doi.org/10.1016/0014-4886(88)90226-9.

[38] Y. Benjamini, D. Drai, G. Elmer, N. Kafkafi, I. Golani, Controlling the false discovery rate in behavior genetics research, Behav. Brain Res. 125 (2001) 279–284. https://doi.org/10.1016/S0166-4328(01)00297-2.

[39] Y. Benjamini, A.M. Krieger, D. Yekutieli, Adaptive linear step-up procedures that control the false discovery rate, Biometrika. 93 (2006) 491–507. https://doi.org/10.1093/biomet/93.3.491.

[40] C. Lois, A. Alvarez-Buylla, Long-distance neuronal migration in the adult mammalian brain, Science (80-.). 264 (1994) 1145–1148. https://doi.org/10.1126/science.8178174.

[41] J.M. Parent, Z.S. Vexler, C. Gong, N. Derugin, D.M. Ferriero, Rat forebrain neurogenesis and striatal neuron replacement after focal stroke, Ann. Neurol. 52 (2002) 802–813. https://doi.org/10.1002/ana.10393.

[42] A. Arvidsson, T. Collin, D. Kirik, Z. Kokaia, O. Lindvall, Neuronal replacement from endogenous precursors in the adult brain after stroke, Nat. Med. 8 (2002) 963–970. https://doi.org/10.1038/nm747.

[43] I. Imayoshi, T. Ohtsuka, D. Metzger, P. Chambon, R. Kageyama, Temporal regulation of Cre recombinase activity in neural stem cells, Genesis. 44 (2006) 233–238. https://doi.org/10.1002/dvg.20212.

[44] S. Srinivas, T. Watanabe, C.S. Lin, C.M. William, Y. Tanabe, T.M. Jessell, F. Costantini, Cre reporter strains produced by targeted insertion of EYFP and ECFP into the ROSA26 locus., BMC Dev. Biol. 1 (2001) 4. https://doi.org/10.1186/1471-213x-1-4.

[45] N. Kaneko, M. Sawada, K. Sawamoto, Mechanisms of neuronal migration in the adult brain, J. Neurochem. 141 (2017) 835–847. https://doi.org/10.1111/jnc.14002.
[46] F. Doetsch, J.M. García-Verdugo, A. Alvarez-Buylla, Cellular Composition and Three-Dimensional Organization of the Subventricular Germinal Zone in the Adult Mammalian Brain, J. Neurosci. 17 (1997) 5046–5061. https://doi.org/10.1523/JNEUROSCI.17-13-05046.1997.
[47] R. Boni, A. Ali, A. Shavandi, A.N. Clarkson, Current and novel polymeric biomaterials for neural tissue engineering, J. Biomed. Sci. 25 (2018) 90. https://doi.org/10.1186/s12929-018-0491-8.
[48] M. Shikanai, K. Nakajima, T. Kawauchi, N-Cadherin regulates radial glial fiber-dependent migration of cortical locomoting neurons, Commun. Integr. Biol. 4 (2011) 326–330. https://doi.org/10.4161/cib.4.3.14886.
[49] A. Kriegstein, A. Alvarez-Buylla, The glial nature of embryonic and adult neural stem cells., Annu. Rev. Neurosci. 32 (2009) 149–184. https://doi.org/10.1146/annurev.neuro.051508.135600.
[50] Y. Yagita, T. Sakurai, H. Tanaka, K. Kitagawa, D.R. Colman, W. Shan, N-cadherin mediates interaction between precursor cells in the subventricular zone and regulates further differentiation, J. Neurosci. Res. 87 (2009) 3331–3342. https://doi.org/10.1002/jnr.22044.
[51] E. Porlan, B. Martí-Prado, J.M. Morante-Redolat, A. Consiglio, A.C. Delgado, R. Kypta, C. López-Otín, M. Kirstein, I. Fariñas, MT5-MMP regulates adult neural stem cell functional quiescence through the cleavage of N-cadherin, Nat. Cell Biol. 16 (2014) 629–638. https://doi.org/10.1038/ncb2993.
[52] M.F. Paredes, D. James, S. Gil-Perotin, H. Kim, J.A. Cotter, C. Ng, K. Sandoval, D.H. Rowitch, D. Xu, P.S. McQuillen, J.M. Garcia-Verdugo, E.J. Huang, A. Alvarez-Buylla, Extensive migration of young neurons into the infant human frontal lobe, Science (80-.). 354 (2016). https://doi.org/10.1126/science.aaf7073.
[53] A. Denoth-Lippuner, S. Jessberger, Formation and integration of new neurons in the adult hippocampus, Nat. Rev. Neurosci. 22 (2021) 223–236. https://doi.org/10.1038/s41583-021-00433-z.
[54] V. Capilla-Gonzalez, V. Herranz-Pérez, J.M. García-Verdugo, The aged brain: genesis and fate of residual progenitor cells in the subventricular zone, Front. Cell. Neurosci. 9 (2015). https://doi.org/10.3389/fncel.2015.00365.
[55] M.P. Jurkowski, L. Bettio, E. K. Woo, A. Patten, S.-Y. Yau, J. Gil-Mohapel, Beyond the Hippocampus and the SVZ: Adult Neurogenesis Throughout the

Brain, Front. Cell. Neurosci. 14 (2020). https://doi.org/10.3389/fncel.2020.576444.
[56] A. Quiñones-Hinojosa, N. Sanai, M. Soriano-Navarro, O. Gonzalez-Perez, Z. Mirzadeh, S. Gil-Perotin, R. Romero-Rodriguez, M.S. Berger, J.M. Garcia-Verdugo, A. Alvarez-Buylla, Cellular composition and cytoarchitecture of the adult human subventricular zone: A niche of neural stem cells, J. Comp. Neurol. 494 (2006) 415–434. https://doi.org/10.1002/cne.20798.
[57] M. Akter, N. Kaneko, V. Herranz-Pérez, S. Nakamura, H. Oishi, J.M. García-Verdugo, K. Sawamoto, Dynamic Changes in the Neurogenic Potential in the Ventricular–Subventricular Zone of Common Marmoset during Postnatal Brain Development, Cereb. Cortex. 30 (2020) 4092–4109. https://doi.org/10.1093/cercor/bhaa031.
[58] N. Sanai, T. Nguyen, R.A. Ihrie, Z. Mirzadeh, H.-H. Tsai, M. Wong, N. Gupta, M.S. Berger, E. Huang, J.-M. Garcia-Verdugo, D.H. Rowitch, A. Alvarez-Buylla, Corridors of migrating neurons in the human brain and their decline during infancy, Nature. 478 (2011) 382–386. https://doi.org/10.1038/nature10487.
[59] E.J. Berns, S. Sur, L. Pan, J.E. Goldberger, S. Suresh, S. Zhang, J.A. Kessler, S.I. Stupp, Aligned neurite outgrowth and directed cell migration in self-assembled monodomain gels, Biomaterials. 35 (2014) 185–195. https://doi.org/10.1016/j.biomaterials.2013.09.077.
[60] V.M. Tysseling-Mattiace, V. Sahni, K.L. Niece, D. Birch, C. Czeisler, M.G. Fehlings, S.I. Stupp, J.A. Kessler, Self-assembling nanofibers inhibit glial scar formation and promote axon elongation after spinal cord injury, J. Neurosci. 28 (2008) 3814–3823. https://doi.org/10.1523/JNEUROSCI.0143-08.2008.
[61] E. Fong, D.A. Tirrell, Collective Cell Migration on Artificial Extracellular Matrix Proteins Containing Full-Length Fibronectin Domains, Adv. Mater. 22 (2010) 5271–5275. https://doi.org/10.1002/adma.201002448.
[62] S. Grade, Y.C. Weng, M. Snapyan, J. Kriz, J.O. Malva, A. Saghatelyan, Brain-Derived Neurotrophic Factor Promotes Vasculature-Associated Migration of Neuronal Precursors toward the Ischemic Striatum, PLoS One. 8 (2013). https://doi.org/10.1371/journal.pone.0055039.
[63] S. Srinivas, T. Watanabe, C.S. Lin, C.M. William, Y. Tanabe, T.M. Jessell, F. Costantini, Cre reporter strains produced by targeted insertion of EYFP and ECFP into the ROSA26 locus., BMC. 1 (2001) 4. https://doi.org/10.1186/1471-213x-1-4.

[64] C. V. Borlongan, T.S. Randall, D.W. Cahill, P.R. Sanberg, Asymmetrical motor behavior in rats with unilateral striatal excitotoxic lesions as revealed by the elevated body swing test, Brain Res. 676 (1995) 231–234. https://doi.org/10.1016/0006-8993(95)00150-O.

Figures & legends

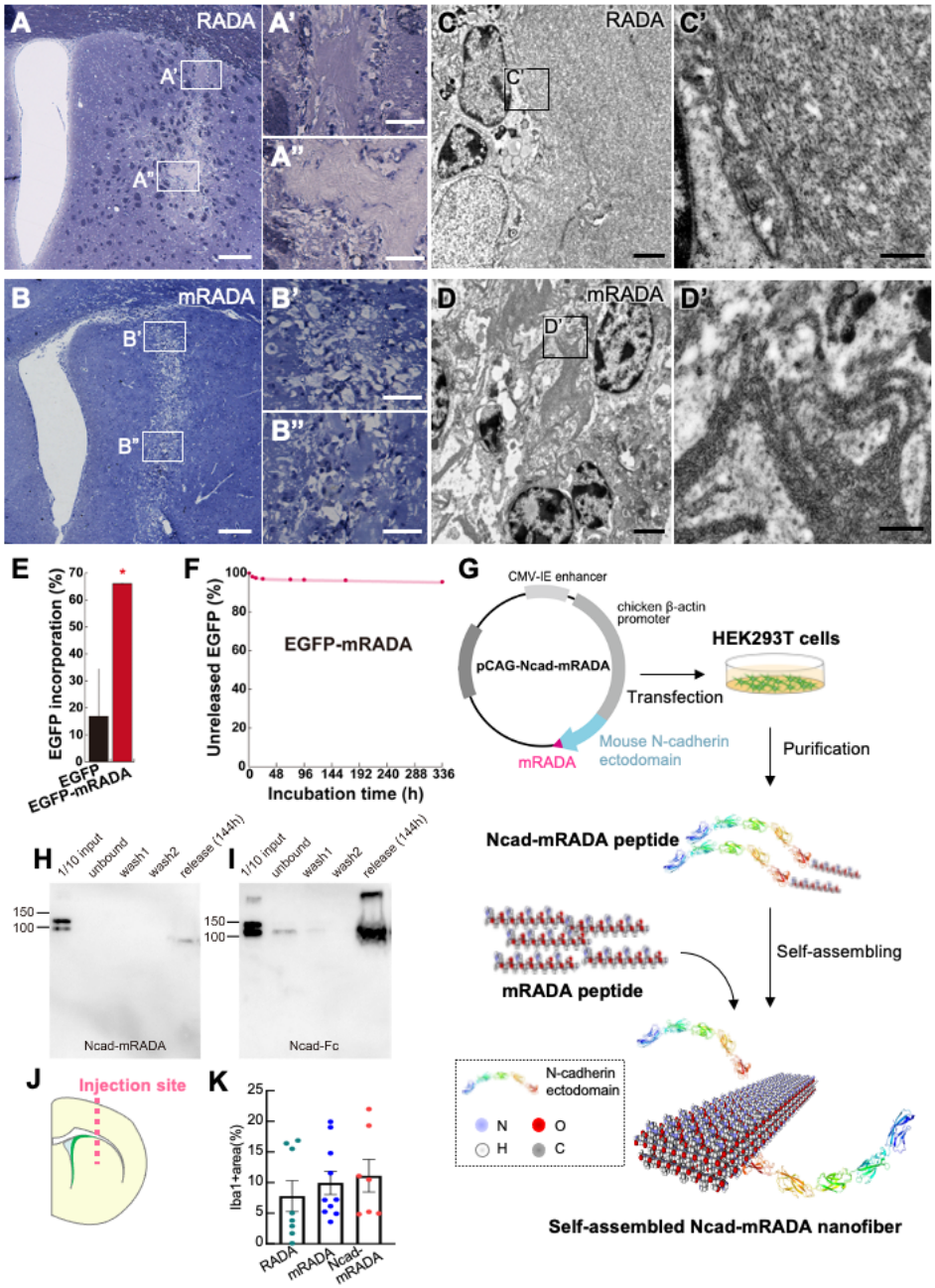

Fig. 1: Ncad-mRADA stably incorporates in mRADA supramolecular hydrogel

A–D: Hydrogel formations of RADA and mRADA peptides injected into intact adult mouse brains. Under light microscopy, semi-thin brain sections embedded in resin show formation of RADA (A) and mRADA (B) hydrogels in the striatum 5 days after injection. A', A", B' and B" are higher magnification images of the boxed areas in A and B. Electron microscopy images of the RADA (C) and mRADA (D) hydrogels in the striatum. C' and D' show higher magnification images of the boxed areas in C and D.

E: The incorporation ratios of non-tagged EGFP and mRADA-tagged EGFP. Protein incorporation (%) = [(weight of input) – (weight of the soluble fraction)] / (weight of input) × 100 (%). *n*=3. Student's t-test.
F: The ratios of unreleased EGFP to incorporated EGFP. Unreleased protein / incorporated protein (%) = [(weight of incorporated protein) – (total weight of the soluble fraction)] / (weight of incorporated protein) × 100 (%). *n* = 3.
G: Scheme of Ncad-mRADA nanofiber production. A plasmid encoding mRADA peptide attached to the N-cadherin extracellular domain sequence was constructed. 293T cells were transfected with the Ncad-mRADA-expressing plasmid. Purified and concentrated Ncad-mRADA proteins were incubated with mRADA. The crystal structure of the mouse N-cadherin extracellular domain was obtained from PDB3Q2W.
H–I: Western blots for released Ncad-mRADA (H) and Ncad-Fc (I) after incubation for 144 h.
J: Experimental design using intact adult mice. Schematic image of a coronal brain section shows material injection site (dotted pink line).
K: Immunological responses to the transplanted biomaterials. The RADA, mRADA, or Ncad-mRADA self-assembling peptides were injected into the striatum of intact adult mice, and brain sections were prepared 5 days later. The graph shows the percentage microglial marker Iba1+ area within 300 μm from the transplanted materials, which was not significantly different among these biomaterials. RADA, *n*=8; mRADA, *n*=10; Ncad-mRADA, *n*=7. One-way ANOVA followed by Bonferroni post hoc test.
Graphs show the mean ± SEM. **p*<0.05. Scale bars: 200 μm, A and B; 50 μm, A', A'', B' and B''; 2 μm, C and D; 0.5 μm, C' and D'.

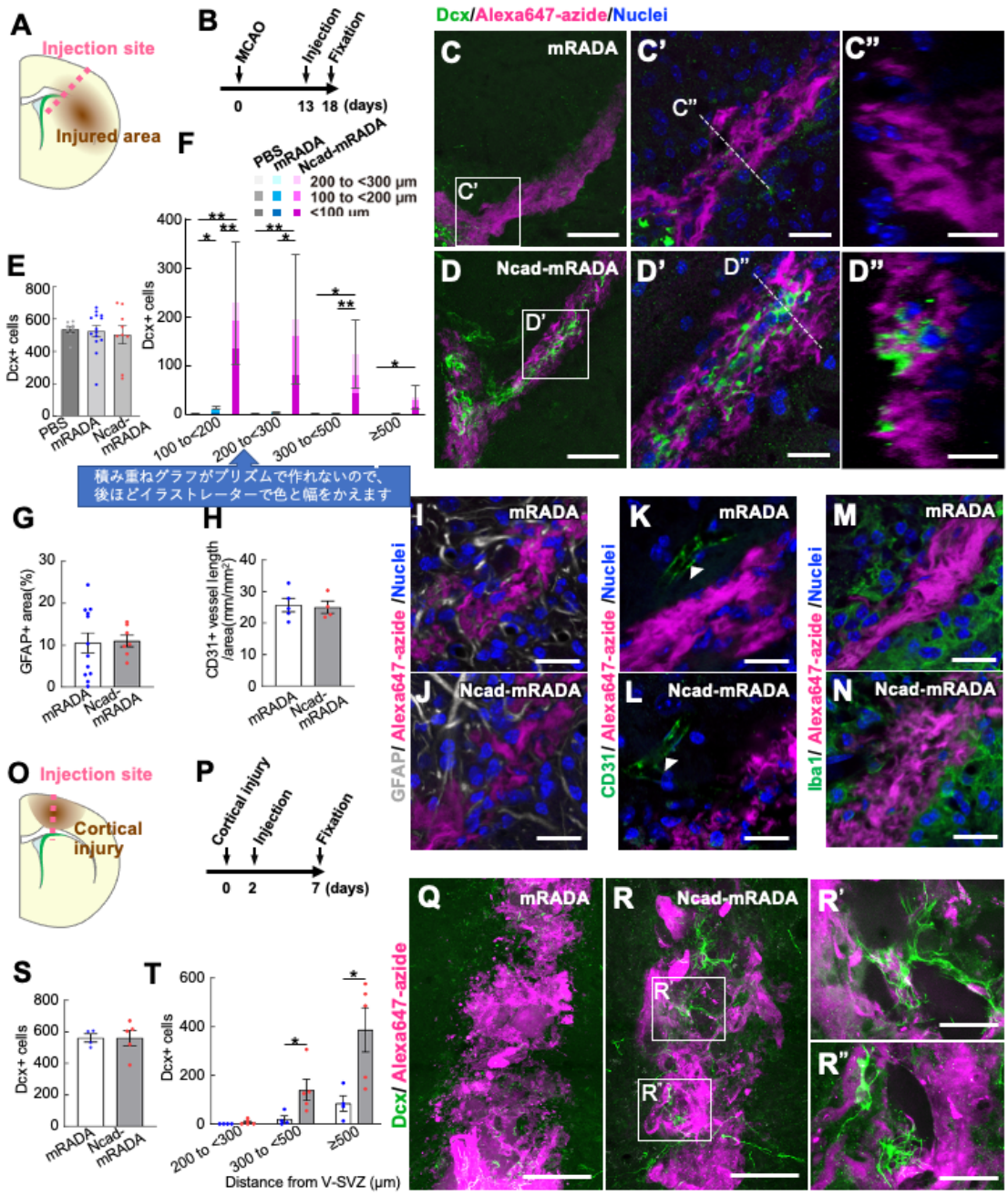

Fig. 2: Ncad-mRADA promotes neuroblast migration toward the injured area in the adult brain

A–B: Experimental design using a cerebral stroke model. Schematic image of a coronal brain section after middle cerebral artery occlusion (MCAO) shows locations of the infarct area (brown area), the V-SVZ (green line) and the injection site (dotted pink line) (A). Timeline of the experimental procedures is shown in (B).

C–F: Distribution of neuroblasts in the brain after stroke followed by PBS, mRADA or Ncad-mRADA injection. Z-stack projection images of the mRADA injection sites in the striatum from coronal brain sections immunostained for neuroblast marker Dcx (C–D

green). mRADA and Ncad-mRADA hydrogels were visualized with AlexaFluor 647-conjugated azide (Alexa647-azide, magenta). Nuclei were labeled with Hoechst 33342. C' and D' are single-plane higher magnification images of the boxed areas in C and D, respectively. C" and D" show cross-section images of the areas indicated in C' and D' (white dotted lines), respectively. The graphs show the numbers of Dcx+ neuroblasts in the V-SVZ (E, per section), and those in areas of post-stroke striatum at different distances (100 to <200 μm, 200 to <300 μm, 300 to <500 μm, and ≥500 μm) from the V-SVZ (F, per mouse). The neuroblasts <100 μm (bottom), 100 to <200 μm (middle) and 200 to <300 μm (top) from PBS, n=8; mRADA, n=14; Ncad-mRADA, n=9) injection sites were separately counted. One-way ANOVA followed by Bonferroni post hoc test. (E) and Wilcoxon rank sum test (F).

G–H: Quantification of distributed non-neuronal cells in the vicinity of mRADA or Ncad-mRADA injection sites. The graphs show percentages of astrocyte marker GFAP+ area within 100 μm from mRADA (n=12) or Ncad-mRADA (n=7) injection sites (G) and quantification of total endothelial cell marker CD31+vascular length per area analyzed within 100 μm from mRADA (n=5) or Ncad-mRADA (n=4) injection sites (H). Student's t-test (G and H).

I–N: Single-plane images of the injection sites in the striatum of coronal brain sections immunostained for GFAP (I and J, white), CD31 (K and L, green) and microglial marker Iba1 (M and N, green). Blood vessels are indicated by white arrowheads.

O–P: Experimental design of the cortical injury model. Schematic image of a coronal brain section after cryogenic injury shows locations of the lesion site (brown area), the V-SVZ (green line) and the material injection site (dotted pink line) (O). Timeline of the experimental procedures is shown in (P).

Q–T: Distribution of neuroblasts in the brain after cortical injury and biomaterial injection. Z-stack projection images of the mRADA injection sites in the cortex from coronal brain sections immunostained for neuroblast marker Dcx (green) at five days after material injection (Q–R). mRADA and Ncad-mRADA hydrogels were visualized with AlexaFluor 647-conjugated azide (Alexa647-azide, magenta). R'-R'' are higher magnification images of the boxed areas in R. The graphs show the numbers of Dcx+ neuroblasts in the V-SVZ (S, per section), and those in areas of injured cortex at different distances (200 to <300 μm, 300 to <500 μm, and ≥500 μm) from the V-SVZ (T, per mouse). The neuroblasts <100 μm (bottom), 100 to <200 μm (middle) and 200 to <300 μm (top) from mRADA, n=4; Ncad-mRADA, n=5) injection sites were separately counted. Student's t test (S and T, 300 to <500 μm, ≥500 μm) and Wilcoxon rank sum test (T, 200 to <300 μm).

Graphs show the mean ± SEM. *p<0.05, **p<0.01. Scale bars: 100 µm, Q–R; 40 µm, C–D; 30 µm, R'–R''; 20 µm, C'–D' and I–N; 10 µm, C''–D''.

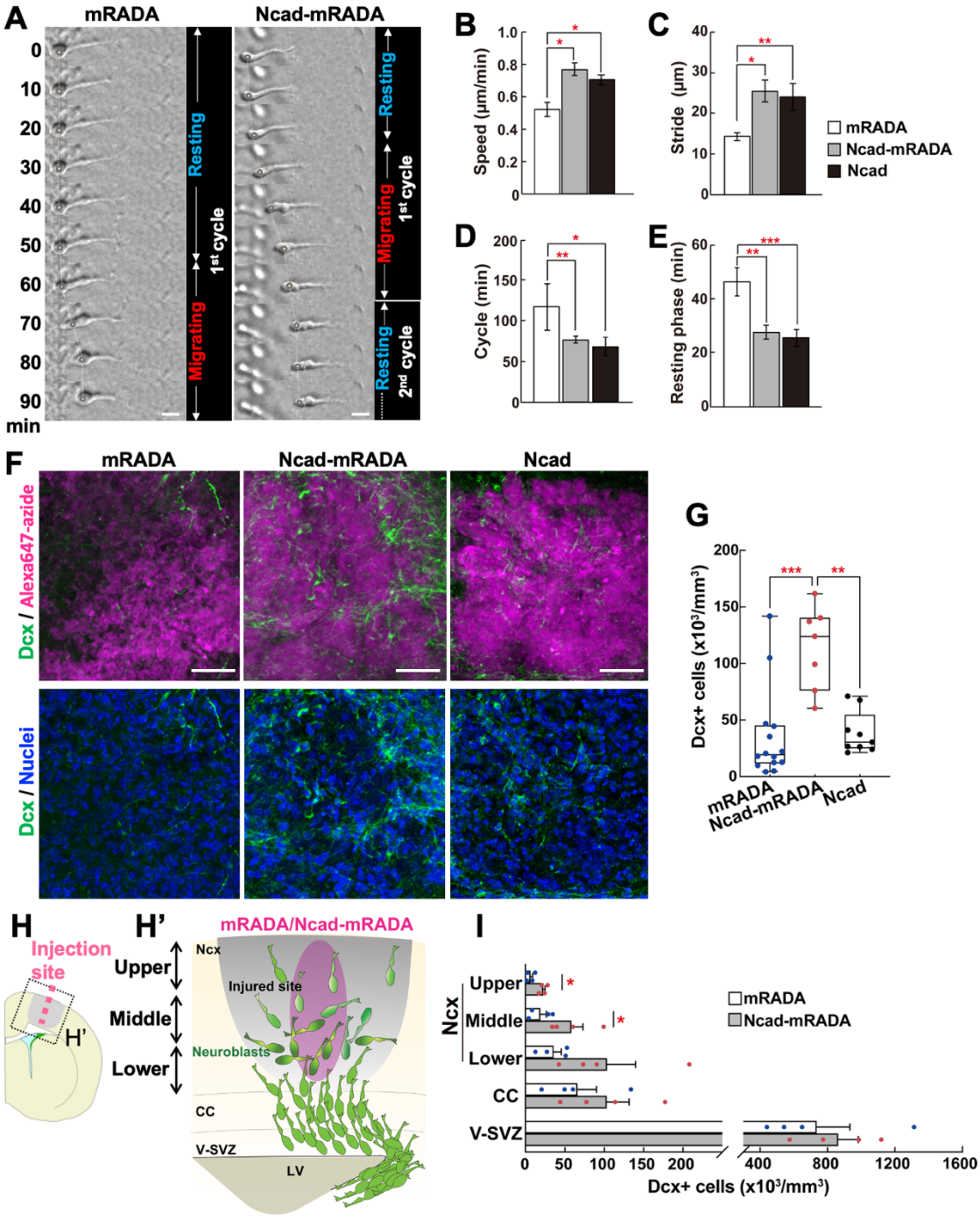

Fig. 3: Ncad-mRADA enhances neuroblast migration towards injured neocortex

A–E: Migration profiles of neuroblasts in contact with the biomaterials. Light microscopy images of neuroblasts migrating on an mRADA or Ncad-mRADA hydrogel-coated dish at different time-points (A). The graphs show quantitative data of migrating speed (B), distance of stride (C), duration of migrating cycle (D), and duration of resting period (E) of neuroblasts on dishes coated with mRADA hydrogel, Ncad-mRADA hydrogel or mRADA hydrogel mixed with Fc domain-conjugated N-cadherin extracellular domain (Ncad hydrogel). At least two independent cultures prepared on different days were used for the analyses. Data are the mean ± SEM. n=9–10 cells each. Kruskal-Wallis test with Steel-Dwass test.

F–G: Distribution of neuroblasts in hydrogels formed in the injured neocortex. Z-stack projection image of Dcx+ neuroblasts (green) distributed inside the mRADA hydrogel, Ncad-mRADA hydrogel or mRADA hydrogel mixed with Ncad-Fc (Ncad hydrogel) four days after injection (F). The mRADA hydrogels were visualized with Alexa647-conjugated azide (Alexa647-azide, magenta). The graph shows the density of Dcx+ neuroblasts inside these mRADA hydrogels (G). Data are represented as box and whisker plots with individual data points. mRADA, n=14; Ncad-mRADA, n=7; Ncad, n=9. Kruskal-Wallis test with Steel-Dwass test.

H–I: Distribution of neuroblasts in neocortex layers after injury. Schematic image shows coronal brain sections with cortical injury (gray) and the injection site (dotted pink line) (H). Magnified schematic diagram of the boxed area in (H) describes neuroblasts (green) migrating from the V-SVZ toward the injured neocortical layers (lower, middle and upper) in the hydrogel (magenta) (H'). The graph shows the density of Dcx+ neuroblasts in the dorsal V-SVZ, corpus callosum (CC), and neocortical layers (lower, middle and upper, indicated in H') at four days after injection of mRADA or Ncad-mRADA (I). Data are the mean + SEM with individual data points. n=4, each. Students' t-test.

*p<0.05, **p<0.01, ***p<0.001. Scale bars: 10 μm, A; 50 μm, F.

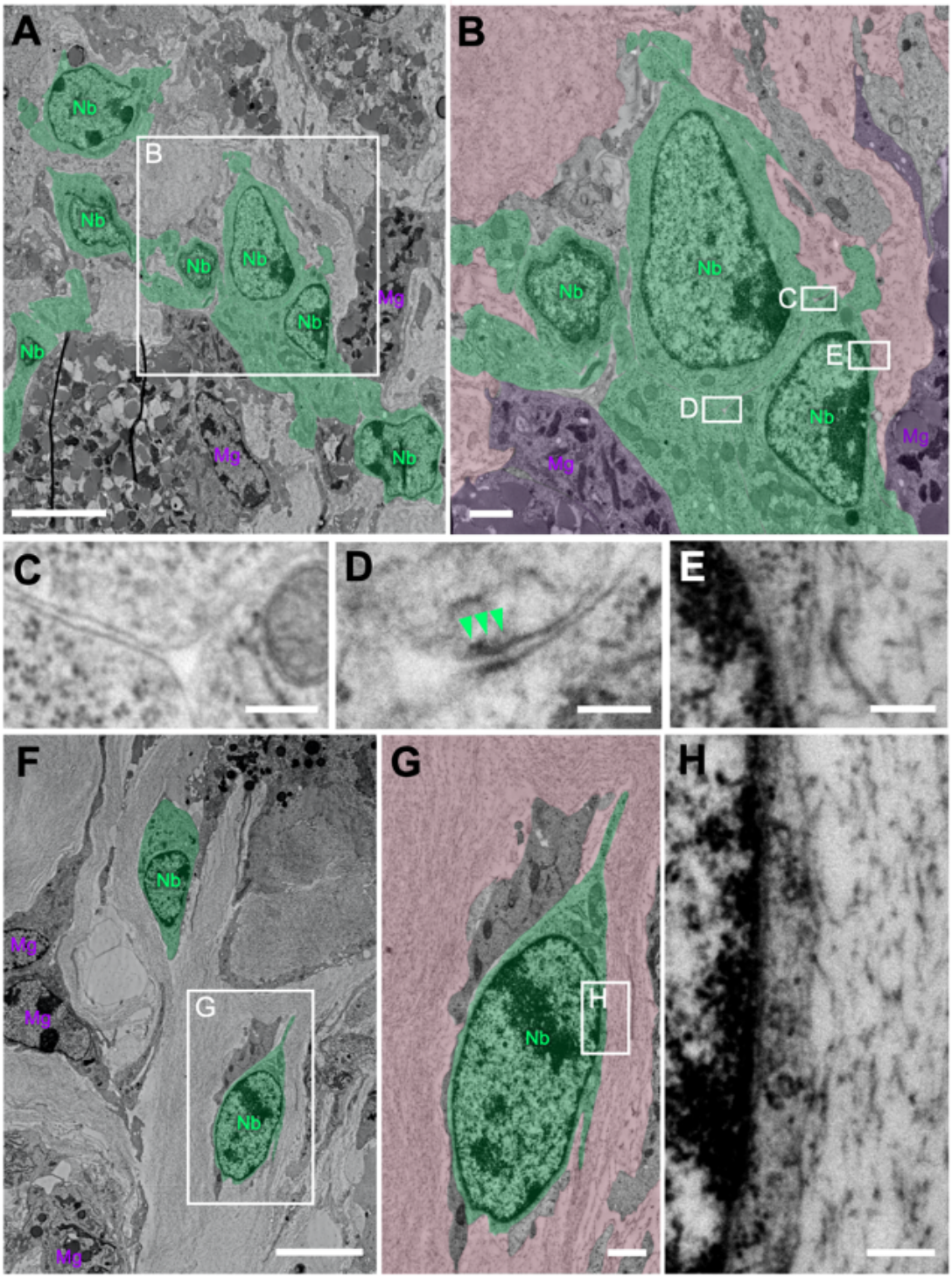

1

Fig. 4: Spatial interactions between neuroblasts and Ncad-mRADA fibers

Transmission electron microscopy of the neonatal neocortex after cryogenic injury and Ncad-mRADA hydrogel injection (A–H). In low magnification images, (A, B, F, G), neuroblasts (Nb) identified by their smooth and elongated cell bodies, small elongated nucleus with lax chromatin and scant cytoplasm containing many free ribosomes and microtubules are colored green. Injury activated microglia (Mg), identified by clumped chromatin in nuclei and many vacuoles and lysosomes in the cytoplasm, are colored purple, and Ncad-mRADA hydrogel is colored pink (B, G). The cluster of neuroblasts directly contact Ncad-mRADA (A, B). Higher magnification images of the boxed areas in B show plasma membrane contact of three neuroblasts (C), adherens-junction like contact (green arrowheads) and free spaces between neuroblasts (D), and direct contact between a neuroblast and Ncad-mRADA fibers (E). Electron micrographs of individual neuroblasts in an Ncad-mRADA hydrogel aggregate show extensive direct contact between neuroblasts and the Ncad-mRADA fibers. G and H are higher magnification images of boxed areas in F and G, respectively.

Scale bars: 5 μm, A, F; 1 μm, B, G; 0.2 μm, C–E, H.

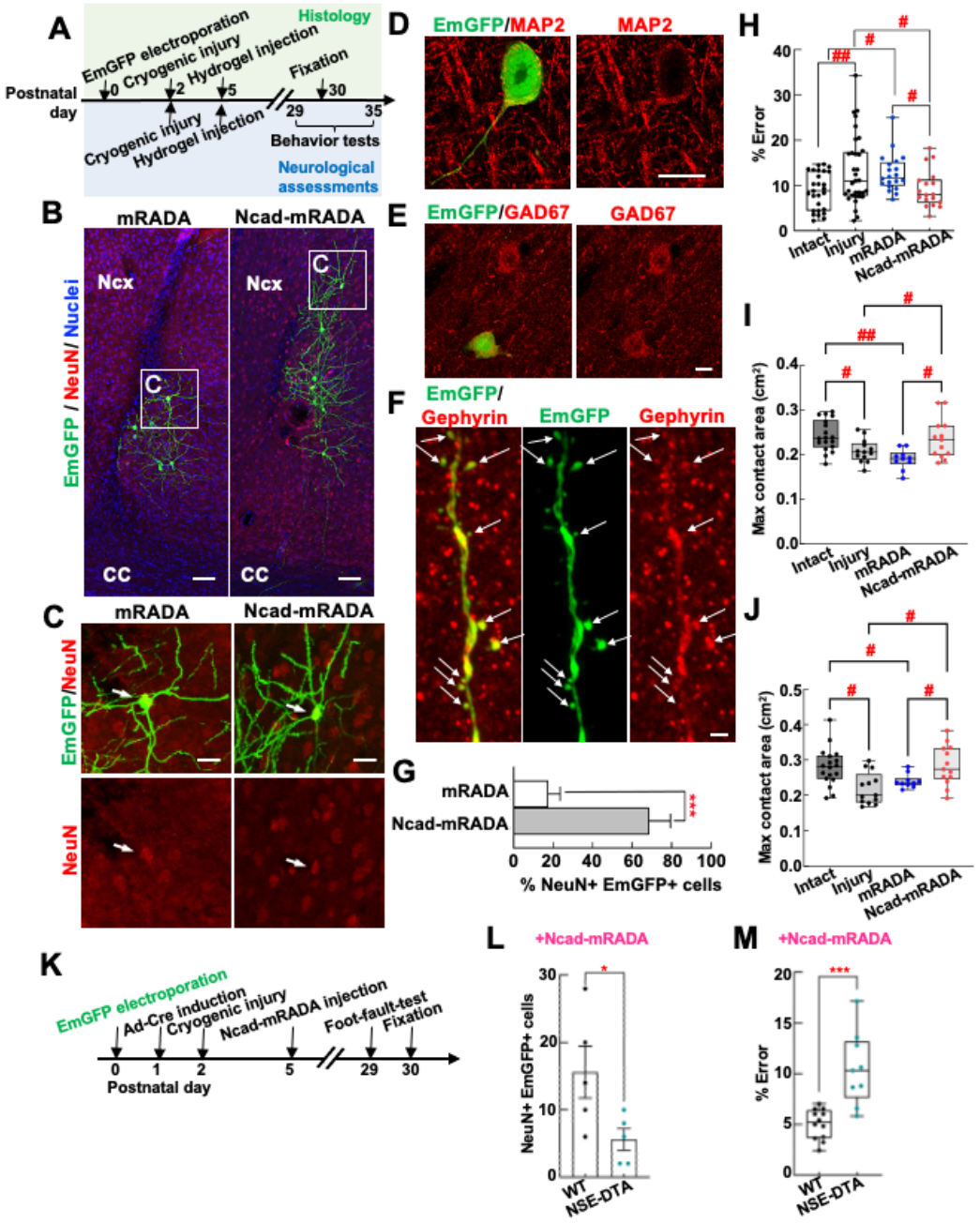

Fig. 5: Ncad-mRADA promotes neuronal regeneration and improves sensorimotor functions during postnatal development

A: Experimental design for labeling V-SVZ-derived cells for histological analyses and neurological assessments.

B–C: Z-stack projection images of coronal brain sections show that EmGFP-labeled (green) V-SVZ-derived cells in the vicinity of the injury express mature neuronal marker NeuN (red). While NeuN+EmGFP+ V-SVZ-derived mature neurons are restricted to the lower layer of the neocortex with mRADA hydrogel, they are distributed more widely

throughout the cortical layers with Ncad-mRADA hydrogel (B). Magnified view of the EmGFP+NeuN+ cells in the boxed areas are presented in C (arrows).
D-F: Single plane image of coronal brain sections show that EmGFP-labeled (green) V-SVZ-derived cell in the injured cortex expresses MAP2 (red) on the soma and a neurite (D). Z-stack projection image of coronal sections show that some V-SVZ-derived cells (green) in the injured cortex express GAD67 (red) (E). Another single plane image indicates the Gephyrin (red) expression on the EmGFP-labelled small protrusions (F).
G: Proportion of EmGFP+NeuN+ cells distributed in the upper layer of the neocortex in mRADA (n=9) and Ncad-mRADA (n=10) groups. Data are the mean + SEM. Welch's t test.
H: Neurological assessments of P29 mice with or without brain injury and a self-assembling peptide injection. The graph represents the percentage of mis-steps (% error) in the foot-fault test. Intact, n=27; injury, n=33; injury followed by mRADA hydrogel treatment (mRADA), n=20; injury followed by Ncad-mRADA hydrogel treatment (Ncad-mRADA), n=18. Data are represented as box and whisker plots with individual data points. One-way ANOVA with Benjamini, Krieger, and Yekutieli FDR test.
I-J: Gait analysis at P33±2.The graph represents "Max contact area" of left forelimb (I) and left hindlimb (J). Intact, n=18; injury, n=13; injury followed by mRADA hydrogel treatment (mRADA), n=10; injury followed by Ncad-mRADA hydrogel treatment (Ncad-mRADA), n=13. Data are represented as box and whisker plots with individual data points. One-way ANOVA with Benjamini, Krieger, and Yekutieli FDR test.
K: Experimental design using *NSE-DTA* mice.
L: Quantification of immunostained EmGFP-labeled V-SVZ-derived cells in the injured cortex expressing NeuN in *NSE-DTA* mice (NSE-DTA, n=5) or wild-type mice (WT, n=5) treated with Cre recombinase followed by cryoinjury and Ncad-mRADA injection. Data are the mean + SEM. Students t-test.
M: Foot-fault test of P29 mice with electroporation, viral induction and cryogenic injury followed by Ncad-mRADA injection. *NSE-DTA*, n=9; WT, n=12. Data are represented as box and whisker plots with individual data points. Students' t-test.
$^{*}p<0.05$, $^{***}p<0.001$, $^{\#}q<0.05$, $^{\#\#}q<0.001$. Scale bars: 50 μm, B; 20 μm, C; 10 μm, D, E; 1 μm, F.

Supplementary Information

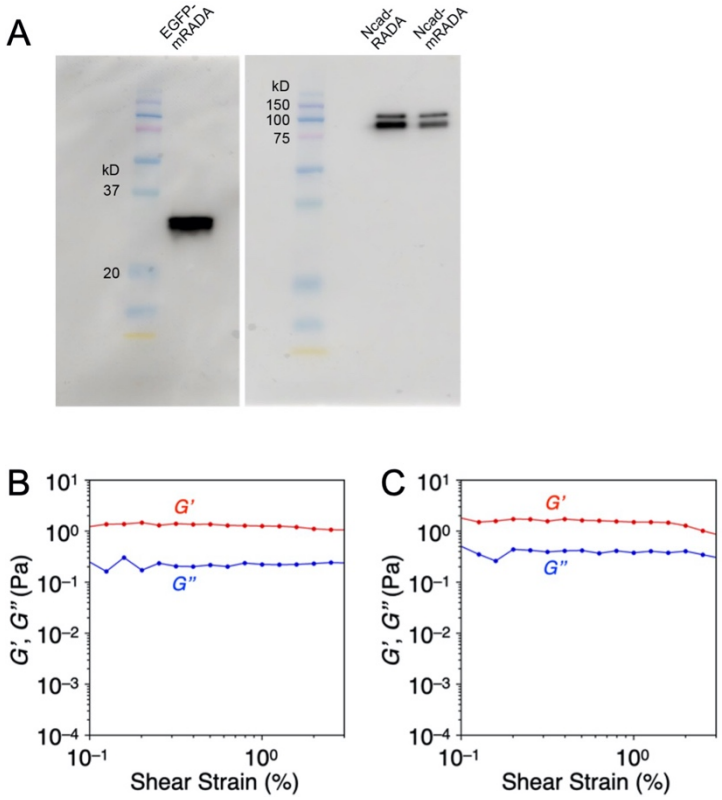

Supplementary Figure 1: Characterization of EGFP-mRADA, Ncad-RADA, and Ncad-mRADA and Rheology of mRADA incorporating Ncad-mRADA

A: Western blotting of EGFP-mRADA (left) and Ncad-RADA and Ncad-mRADA (right). ~~80 pg of EGFP-mRADA and 80 ng of Ncad-RADA and Ncad-mRADA proteins were mixed with SDS loading buffer and subjected to SDS-PAGE on 12% polyacrylamide gels. The proteins were then electroblotted onto polyvinylidene fluoride membranes using an iBlot Gel Transfer Device (Thermo Fisher Scientific). The membranes were incubated with rabbit anti-GFP (1:5,000, ab290, Abcam) and rabbit anti-N cadherin (1:5,000, ab76011, Abcam) for 16 h at 4˚C after blocking with 5% skim milk for 1 h at room temperature, and then with peroxidase-labeled goat anti-rabbit IgG (1:5,000, Dako, Glostrup, Denmark) for 2 h. The bands were detected using SuperSignal West Femto Maximum Sensitivity Substrate (Thermo Fisher Scientific) and were visualized using a Amersham ImageQuant 800 (Cytiva; Tokyo, Japan).~~

B-C: Strain-dependent storage (G', red) and loss (G", blue) moduli profiles of mRADA (B) and a mixture of mRADA and Ncad-mRADA (C) in PBS buffer at 25˚C (mRADA concentration: 0.5 wt%, Ncad-mRADA concentration: 40 ng/μL, pH 3.0).

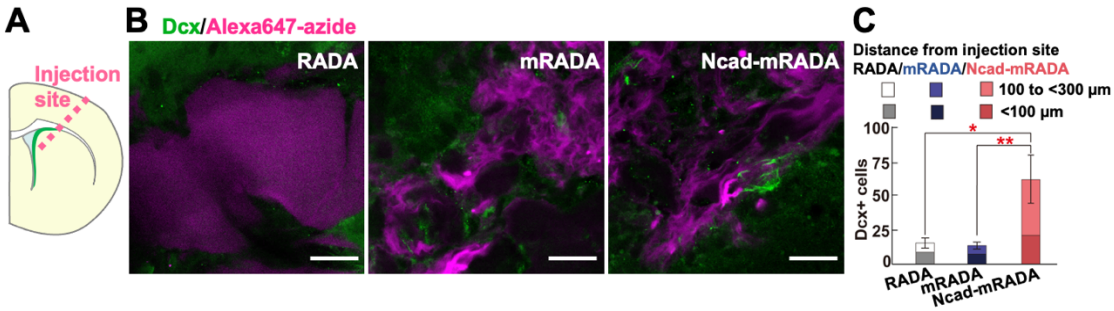

Supplementary Figure 2: Ncad-mRADA injected into the striatum of intact mice contacts more neuroblasts than other materials

A: Schematic image of a coronal brain section shows the V-SVZ (green line) and the injection site (dotted pink line).

B: Distribution of neuroblasts in the intact brain at five days after RADA, mRADA and Ncad-mRADA injection. Single-plane images of the injection site in the striatum from coronal brain sections immunostained for neuroblast marker Dcx (green). RADA, mRADA and Ncad-mRADA hydrogels were visualized with AlexaFluor 647-conjugated azide (Alexa647-azide, magenta).

C: The graph shows the numbers of Dcx+ neuroblasts in the areas of the striatum at different distances from injection sites (<100 µm and 100 to <300 µm) from RADA (n=6), mRADA (n=11) or Ncad-mRADA (n=7) injection sites (per mouse). Kruskal-Wallis test followed by Steel-Dwass test. Graphs show the mean ± SEM.

*p<0.05, **p<0.01. Scale bars: 20 µm, B.

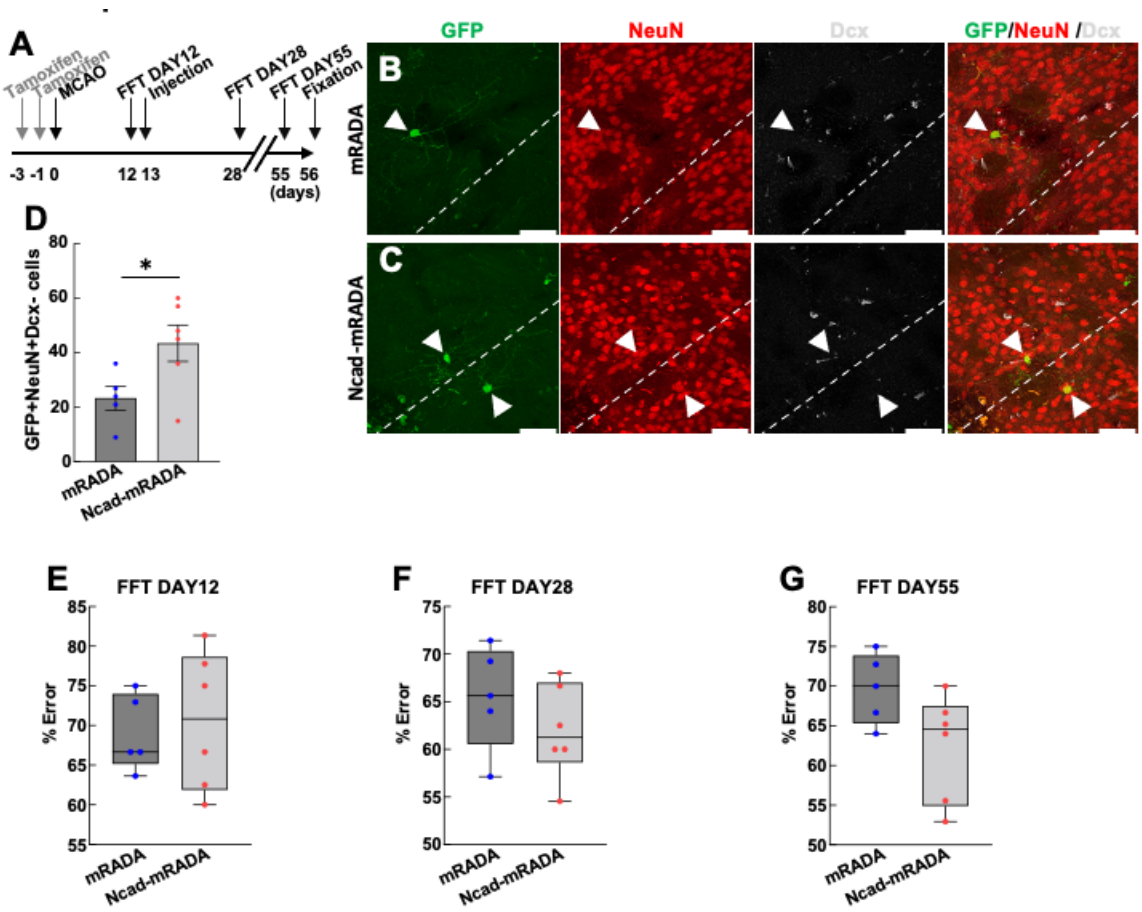

Supplementary Figure 3: Ncad-mRADA increases the number of V-SVZ-derived mature neurons in the post-stroke striatum

A: Experimental design for analyzing maturation of V-SVZ-derived cells in the post-stroke striatum using Nes-CreER;R26R-ECFP transgenic mice.

B-C: Representative images of ECFP-labeled (GFP+, green) cells (white arrows) expressing NeuN (red), but not Dcx (white) around the injection tracks (white dotted lines) of mRADA (B) and Ncad-mRADA (C) at 56 days after MCAO.

D: Quantification of the number of GFP+NeuN+Dcx- cells in the post-stroke striatum within 200 μm from the needle tracks. The number was significantly higher in the Ncad-mRADA group (n=5) compared with the mRADA group (n=6). Student's t test.

E-G: Foot-fault test at 12 days (E), 28 days(F), and 55 days(G) after stroke induction (MCAO). stroke followed by mRADA hydrogel treatment (mRADA), n=5; injury followed by Ncad-mRADA hydrogel treatment (Ncad-mRADA), n=6. Data are represented as box and whisker plots with individual data points. Student's t test.

Graphs show the mean ± SEM. *p<0.05. scale bars: 50μm

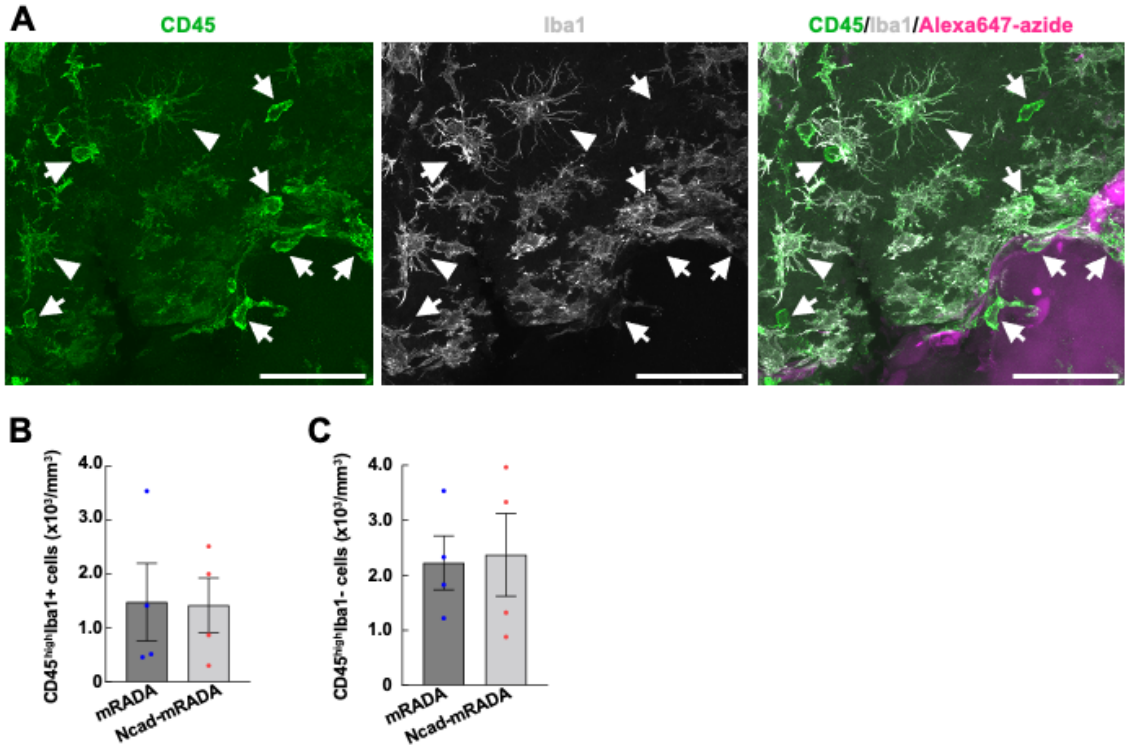

Supplementary Figure 4: Ncad-mRADA does not affect immune cell infiltration in the post-stroke striatum

A: Representative images of infiltrated blood cells around the mRADA hydrogel in the post-stroke brain. The brain sections 18 days after MCAO were immunostained for general leukocyte CD45 (green) and macrophage/microglial marker for Iba1 (white). The mRADA hydrogel was visualized with AlexaFluor 647-conjugated azide (Alexa647-azide, magenta). White arrowheads and arrows indicate leukocytes that express CD45 at high level ($CD45^{high}$) with and without expressing Iba1, respectively.

B-C: Quantification of leukocytes infiltrated around the mRADA and Ncad-mRADA hydrogels. The graphs show the density of $CD45^{high}$Iba1+ cells (macrophages, B) and $CD45^{high}$Iba1- cells (subtypes of leukocytes other than macrophages, C) in the striatum within 300μm from the injection track of mRADA (n=4) or Ncad-mRADA (n=4). There were no significant differences in both of the cell densities between the groups. Student's t test. Graphs show the mean ± SEM.

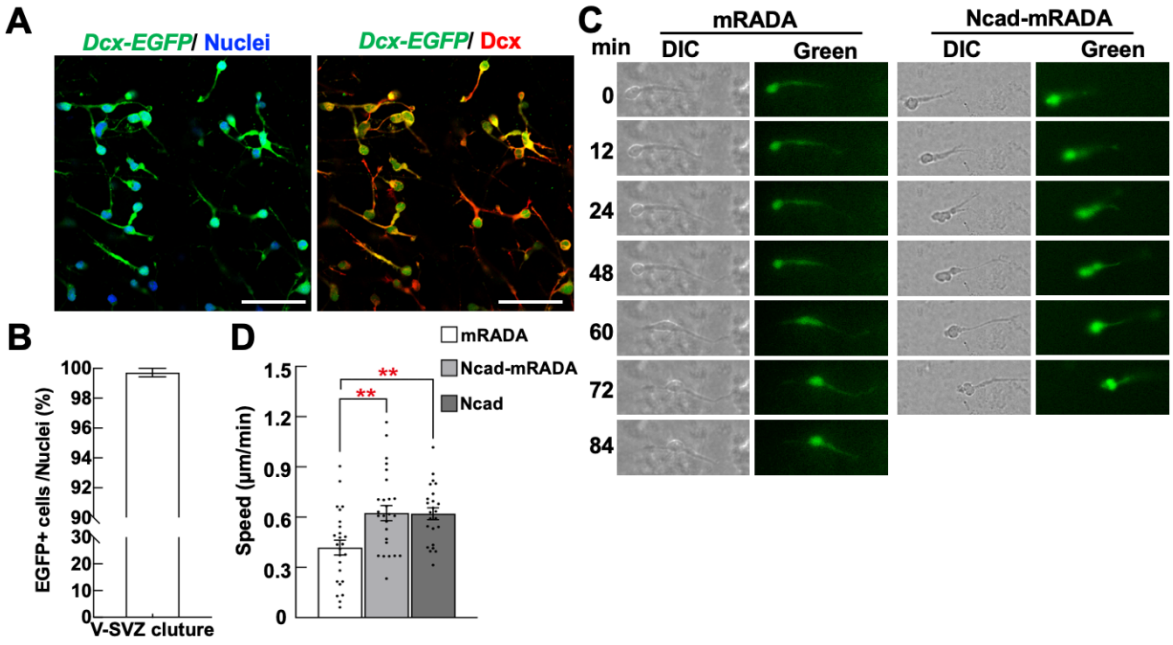

Supplementary Figure 5: N-cadherin containing mRADA peptides promote migration of GFP-labeled neuroblasts derived from Dcx-EGFP mouse V-SVZ

A: Representative image of the day 3 in vitro V-SVZ culture using Dcx-EGFP mice. Dcx-EGFP+ (green) cells were immunostained for Dcx (red) and GFP (green) and counter stained with Hoechst33342 (blue).

B: Quantitative analysis of the Dcx-EGFP+ cells from the day 3 *in vitro* V-SVZ culture shown in percentage. Graph shows the mean ± SEM.

C-D: DIC and Green fluorescence images of migrating Dcx-EGFP+ cells on an mRADA or Ncad-mRADA hydrogel-coated dish at different time-points (C). The graph shows quantitative data of migrating speed of neuroblasts on dishes coated with mRADA hydrogel, Ncad-mRADA hydrogel or mRADA hydrogel mixed with Fc domain-conjugated N-cadherin extracellular domain (Ncad hydrogel, Ncad) (D). At least two independent cultures prepared on different days were used for the analyses. Data are the mean ± SEM. mRADA, n=25; Ncad-mRADA, n=27; Ncad, n=24 cells each. One-way ANOVA followed by Bonferroni post hoc test. **p<0.01. Scale bar: 50 μm, A.

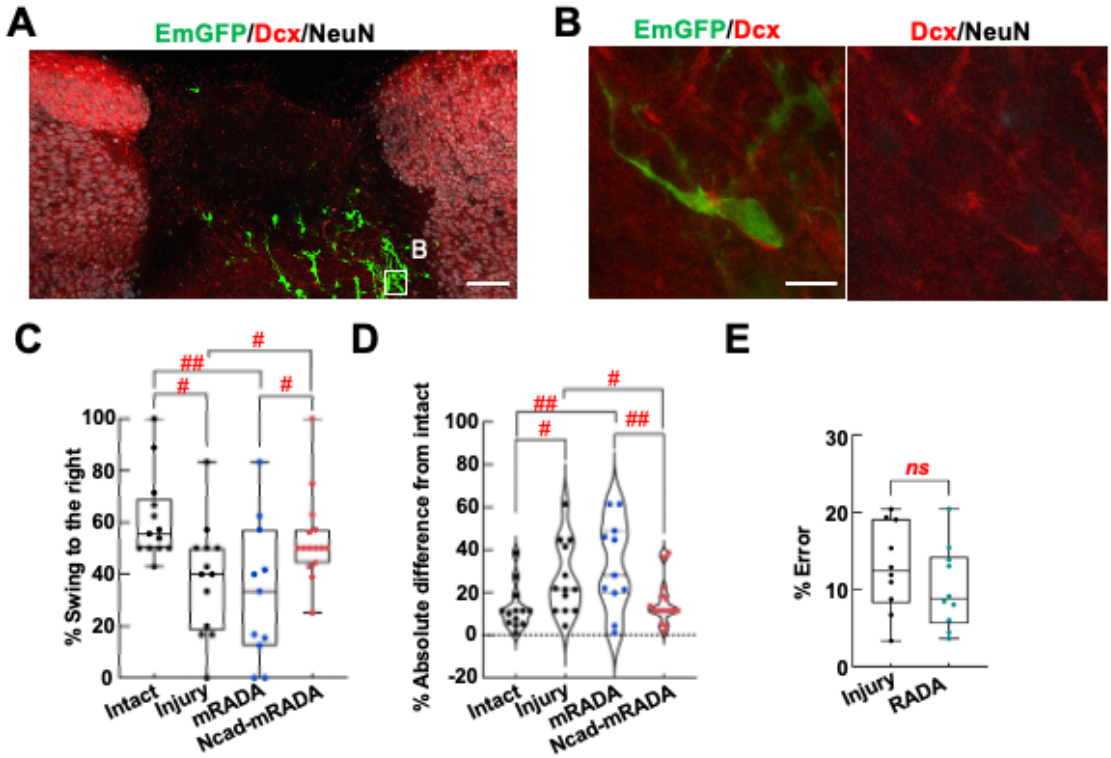

Supplementary Figure 6: Ncad-mRADA peptide treatment promotes sensorimotor recovery in mice after neonatal cortical injury

A-B: Coronal brain sections of wild-type mice after electroporation of *EmGFP*-encoding plasmid at P0, neocortical injury at P2 and Ncad-mRADA injection at P5, and fixation at P9 were immunostained for Dcx and NeuN. The EmGFP-labeled V-SVZ-derived cell (green) are distributed in the injured tissue where NeuN+ mature neurons (white) are lost (A). A high magnification image of boxed area in (A) shows EmGFP-labeled cell (green) in injured cortex expressing Dcx (red), but not NeuN (white) (B).

C-D: Elevated body swing test (EBST) on P30 mice with or without brain injury and a self-assembling peptide injection. The graph represents the percentage of right swings (% Swing to the right) in the EBST (C). The absolute differences of the percentage of right swing in each mouse from that of the average value in intact group was quantified and plotted (D). Intact, n=13; injury, n=13; injury followed by mRADA hydrogel treatment (mRADA), n=11; injury followed by Ncad-mRADA hydrogel treatment (Ncad-mRADA), n=15. Data are represented as box and whisker plots (C) and as violin plots (D) with individual data points. One-way ANOVA with Benjamini, Krieger, and Yekutieli FDR test.

E: Foot-fault test on P31 mice with or without RADA injection after cryogenic injury. Injury, n=10; RADA, n=10. Students' t-test.

$ns \geq 0.05$, $^{\#}q<0.05$, $^{\#\#}q<0.001$. Scale bars: 100 µm, A; 10 µm, B.

Supplementary Movie 1: Time-lapse imaging of cultured neuroblasts migrating on mRADA and Ncad-mRADA hydrogels

The behavior of migrating neuroblasts was recorded at 1-min intervals. Sequential images of these neuroblasts are shown in Figure 3A.

Materials and Methods for Supplementary Data

Ncad-mRADA injected into the striatum of intact mice contacts more neuroblasts than other materials

Eight-to-ten-week-old male mice were anesthetized and subjected to the following procedures. Prior to injection of the synthesized peptide solution, scalp and parietal bone near the injection sites were resected to expose the brain. Peptide solution (2.5 μl) was injected into the intact medial striatum (1.55 mm anterior, 0.8 mm lateral to bregma, 1.50–3.0 mm deep).

The mice were transcardially perfused 5 days after the material injection with phosphate buffered saline (PBS, pH 7.4), followed by 4% paraformaldehyde (PFA) in 0.1 M phosphate buffer (PB, pH 7.4). Tissues were further fixed in the same fixative overnight. Coronal sections 50 μm thick were then prepared with a vibratome VT1200S (Leica, Wetzlar, Germany). The sections were immunostained for Dcx and injected material was visualized with AlexaFluor 647-conjugated azide.

Images were acquired using an LSM700 confocal microscope equipped with 10×/0.45 and 20×/0.8 objective lenses. Samples with material injection within 200 μm of the V-SVZ were selected and subjected to quantitative analysis. The number of neuroblasts in every third 50-μm-thick coronal section was counted and the neuroblast number was multiplied by three to obtain the total number of cells per animal. The neuroblasts that were closer than 100 μm or 100 to <300 μm from the injection site were analyzed. The area within 100 μm from the V-SVZ was excluded from counting. Mice with RADA (n=6), mRADA (n=11) and Ncad-mRADA (n=7) hydrogels were analyzed (Fig. S2).

Maturation of V-SVZ-derived cells in the post-stroke brain of adult mice

Male adult Nestin-CreER;R26R-ECFP mice obtained by crossing the Nestin-CreER mice [43] and R26R-ECFP transgenic mice [63] described previously were used. Tamoxifen administration induces nuclear transfer of Cre recombinase in nestin promoter active neural stem/progenitor cells, which results in removal of a “floxed” STOP sequence at the Rosa 26 locus, leading to persistent expression of a fluorescent protein ECFP. The mice were injected with tamoxifen (100 mg/kg/day) at three and one days before MCAO operation, then injected with Ncad-mRADA or mRADA at day 13, and fixed at day 56 days after MCAO. The coronal brain sections were immunostained with GFP (rabbit anti-GFP (1:500, MBL, Tokyo, Japan)), Dcx (guinea-pig anti-DCX (1:800, Millipore)) and NeuN (mouse anti-NeuN (1:200, Millipore)) antibodies. Images of the areas with needle tracks of biomaterial injection in the ipsilateral triatum were obtained

using confocal laser microscope (FV3000, Olympus). The number of ECFP-labeled (GFP+) cells expressing NeuN, but not Dcx distributed within 200 μm from the needle tracks were counted (Fig. S3).

Foot-fault test on the post-stroke adult mice

The foot-fault test on adult mice was performed as previously described with modifications [37]. Briefly, mice were placed on elevated hexagonal grids of 40-mm diameter. The mice placed their paws on the wire and moved along the grid. With each weight-bearing step, the paw may fall or slip between the wire; either type of misstep was recorded as a foot-fault. The number of foot-faults for each limb was separately counted for 6 min, and then the percentages of foot faults were calculated as follows. The trials were repeated at 12 days (one day before biomaterial injection), 28 days, and 55 days after stroke induction (MCAO). The mice were trained to walk on the grid for 20 min the day before the trial. The number of left hindlimb foot-faults was divided by the number of the total foot-faults of left and right hindlimb and described in percentage (Fig. S3).

Immunohistochemistry

To examine immune cell infiltration in the brain after biomaterial injection, 18 day-post-stroke brain sections injected with Ncad-mRADA or mRADA were immunostained for general leukocyte marker, CD45 (rat anti-CD45 (1:400, Bio-Rad, California, USA)) and macrophage/microglial marker Iba1(rabbit anti-Iba1 (1:2,000, Wako Pure Chemical Industries, Osaka, Japan)). The hydrogels were visualized with AlexaFluor 647-conjugated azide. Cells expressing CD45 at high level ($CD45^{high}$) were regarded as leukocytes. Using the images of the areas around the hydrogels obtained using confocal laser microscope (FV3000, Evident), the density of $CD45^{high}$ Iba1+ cells (macrophages) and $CD45^{high}$ Iba1- cells (subtypes of leukocytes other than macrophages) were quantified (Fig. S4).

V-SVZ neuroblast culture from *Dcx-EGFP* mice

Glass-bottom 35-mm Petri dishes coated with mRADA, Ncad-mRADA or Ncad hydrogel were prepared prior to cell preparation. The dishes were incubated with the biomaterial solution for 30 min at 4ºC and for a further 30 min at 37ºC. The dishes were rinsed once with PBS and air-dried in a laminar flow hood until use. V-SVZ tissues were dissected from postnatal day 0 *Dcx-EGFP* mice [28] and dissociated with trypsin-EDTA (Thermo Fisher Scientific). The cells were washed with L-15 medium (Thermo Fisher Scientific) containing 20 μg/ml DNaseI (Roche). The cell aggregate was embedded in 50% Matrigel (BD Biosciences, diluted in Hank's balanced salt solution (Thermo Fisher

Scientific). The cells were cultured in Neurobasal medium containing 2% B-27% supplement, 2 mM L-glutamine and 50 U/ml penicillin-streptomycin at 37ºC with 5% CO_2 for 48 h before imaging. Details of the cell preparation is described elsewhere [33]. Time-lapse video recordings were performed using a BZ-X800 fluorescence microscope (Keyence, Osaka, Japan) equipped with a ×20 dry objective lens. Both DIC and green fluorescence images of *Dcx-EGFP*+ cells were obtained every 4 min for 24 h under humidified conditions at 37ºC with 5% CO_2. The migrating *Dcx-EGFP*+ cells were analyzed using a manual tracking plugin of the ImageJ software (National Institutes of Health, Bethesda, MD, USA).

After the time-lapse imaging, the cells were fixed with 4% PFA in PB. The fixed cells were further proceeded with immunostaining. Briefly, the cells were permeabilized and blocked with blocking buffer (10 % normal donkey serum, 0.4% Triton-X100 in PBS) for 1 h and incubated with primary antibody solution containing rat anti-GFP (1:500, Nacalai, Kyoto, Japan) and rabbit anti-DCX (1:500, Cell Signaling Technologies) antibodies in the blocking buffer overnight at 4ºC. Then the cells were washed and stained with anti-rat AlexaFluor488 and anti-rabbit AlexaFluor568 antibodies (1:1,000, Thermo Fisher Scientific) in blocking buffer for 1 h. Cell nuclei were stained with Hoechst 33342 stain (1:5,000, Invitrogen). Images were acquired using an LSM700 confocal microscope equipped with 20×/0.8 objective lens. Images from 5 individual V-SVZ aggregates were obtained and percentage of GFP+ cells/ total Hoechst+ cells was quantified (Fig. S5).

Postnatal V-SVZ labeled cells analysis

To label V-SVZ cells 2 µl plasmid solution (4 µg/ml *pCAGGS-EmGFP* [35] in distilled water containing 0.01% Fast Green) was injected into the lateral ventricle of the right hemisphere of P0 ICR mice using the following stereotaxic coordinates: 2.0 mm anterior, 1.2 mm lateral to lambda and 2.0 mm deep. The animals were subjected to three electrical pulses (70 V, 20.0 msec) using a Super Electroporator NEPA21 Type II (Nepa Gene, Chiba, Japan) and 10 mm tweezer electrodes (CUY650P10, Nepa Gene, Chiba, Japan). Electroporated animals were placed on a heating plate before being returned to their home cage. Next, the electroplated P2 animals were subjected to cryogenic injury. Briefly, a pre-chilled 1.2 mm-wide hexagonal wrench was prepared in liquid nitrogen and was placed on the exposed right skull (0.5-mm anterior and 1.2-mm lateral to lambda) for 10 seconds. The procedure was repeated three times with a time interval of 5 seconds to re-chill the probe. Then P5 animals were subjected to intracortical injection of 2 µl Ncad-mRADA solution into the lesion site (1.0–1.5 mm deep from the skull surface). After the injection, the capillary needle was kept in the injection site for 5–7 min, until hydrogel formation was accomplished. Mice were transcardially perfused 5 days after the injection

with PBS (pH 7.4), followed by 4% paraformaldehyde (PFA) in 0.1 M PB (pH 7.4). Tissues were further fixed in the same fixative overnight. The obtained brain sections were immunostained overnight at 4ºC with the primary antibodies of rat anti-GFP (1:500, Nacalai, Kyoto, Japan), guinea pig anti-DCX (1:800, Millipore) and rabbit anti-NeuN (1:1000, Abcam), followed by secondary antibody solution containing AlexaFluor-conjugated secondary antibodies (1:1,000, Thermo Fisher Scientific) for 2 h at room temperature. Cell nuclei were stained with Hoechst 33342 stain (1:5,000, Invitrogen). Images were acquired using an LSM700 confocal microscope equipped with 20×/0.8 objective lens (Fig. S6).

Elevated body swing test

To analyze the asymmetric motor behavior [17,64] in mice after neonatal cortical injury, P30 wild-type mice after cryogenic injury at P2 with or without following mRADA or Ncad-mRADA peptide injection at P5, or intact mice were subjected to the elevated body swing test (EBST). The mice were acclimated in the procedure room for 20 min before the test. The tail was taken ca. 4 cm from the base and was suspended approximately 10 cm above the table for 90 seconds in the vertical axis. Swings to the left or right was counted when the animal moved its head out of the vertical axis at least 90°. Swings were recorded with the video camera, and the percentage of right swings was determined. The absolute difference between average value of the intact mice and each value was shown in the violin plots (median and first and third quartiles for each group data are shown) (Fig. S6).

Foot-fault test on neonatal cryoinjured mice with or without RADA injection

The foot-fault test was performed as previously described with modifications [37] on cryoinjured P31 ICR mice with or without RADA injection. Briefly, mice roamed on 20-cm elevated hexagonal wire grids with 40-mm diameter openings for 10 min on a day prior to the test. During the test, each mouse was tested for 5 min on the grid and the total number of steps and foot-faults for the left hindlimb were recorded. A misplaced limb that slipped on the grid or fell through the openings in the grid was counted as a foot-fault. The number of foot-faults for the left hindlimb was divided by the total number of hindlimb steps to determine percentage of the fault steps. The test was repeated twice on the same day for each mouse and the percentage of the fault steps averaged (Fig. S6).

Time-lapse imaging of cultured neuroblasts migrating on mRADA and Ncad-mRADA hydrogels

Glass-bottom 35-mm Petri dishes coated with mRADA or Ncad-mRADA hydrogel were prepared prior to cell preparation. The dishes were incubated with the biomaterial solution for 30 min at 4ºC and for a further 30 min at 37ºC. The dishes were rinsed once with PBS and air-dried in a laminar flow hood until use.

V-SVZ tissues were dissected from postnatal day 0 ICR mice and dissociated with trypsin-EDTA (Thermo Fisher Scientific). The cells were washed with L-15 medium (Thermo Fisher Scientific) containing 20 μg/ml DNaseI (Roche). The cell aggregate was embedded in 50% Matrigel (BD Biosciences, diluted in Hank's balanced salt solution (Thermo Fisher Scientific). The cells were cultured in Neurobasal medium containing 2% B-27% supplement, 2 mM L-glutamine and 50 U/ml penicillin-streptomycin at 37ºC with 5% CO_2 for 48 h before imaging. Details of the cell preparation is described elsewhere [33]. Time-lapse video recordings were performed using a BZ-X800 fluorescence microscope (Keyence, Osaka, Japan) equipped with a ×20 dry objective lens. Images of neuroblasts were obtained every 1 min for 24 h under humidified conditions at 37ºC with 5% CO_2 (Movie S1).